Final Master's Thesis

Model cell membranes for biomedical applications.

Author

Lara Adwan Al Chihabi

Supervisors

Pilar Cea Mingueza

Santiago Martín Solans

Physical Chemistry department

Sciences faculty

University of Zaragoza

2023-2024

Table of Contents

Abstract

Analysing the interactions of xenobiotics, pharmaceutical agents, nanoparticles, or other agents with cell membranes is a challenging process, largely due to the structural and functional complexity of cell membranes. To overcome these challenges, fundamental research often employs artificially assembled model cell membranes, which allow precise control over their composition and properties. In this Final Master's thesis, the Langmuir technique is used to model the plasma membrane of healthy and inflammatory bowel disease-affected colonocytes at the air-water interface. These model membranes are used to investigate their interactions with [6]-Gingerol, a xenobiotic well-known for its antioxidant, anti-inflammatory, and antitumoral properties as well as its protective role in patients with inflammatory bowel disease (IBD). However, the low water solubility of [6]-Gingerol severely restricts its bioavailability, and thus its use as a therapeutic agent. This Final Master's objective is to gather information about the molecular interactions between [6]-Gingerol and the components of plasma membranes, which could lay the groundwork for future development of delivery systems (e.g. liposomes or artificial exosomes) aimed at enhancing the therapeutic potential of [6]-Gingerol. In addition, the analysis of the interactions of [6]-Gingerol with healthy and disturbed model cell membranes could also contribute to a better understanding of the therapeutic effect of this xenobiotic. The influence of [6]-Gingerol in membrane fluidity, stability, and thermodynamic properties was assessed through the data retrieved from surface pressure-area per molecule isotherms. Results indicate that higher χ_{GIN} values increase membrane fluidity. From a thermodynamic point of view, both systems exhibit repulsive interactions between [6]-Gingerol and membrane components, which are generally stronger in the healthy membrane (HM). Incorporation of [6]-Gingerol into both model membranes was also studied using adsorption experiments in which surface pressure measurements were analysed, and by means of the *in situ* visualization of the monolayers at the air-water interface using Brewster Angle Microscopy (BAM). In conclusion, [6]-Gingerol is capable of penetrating both model membranes, exhibiting a more favourable incorporation in the HM membrane as opposed to the IBD-affected one. All these findings highlight the distinct thermodynamic and structural behaviour of [6]-Gingerol interactions with healthy versus IBD-affected membrane models, contributing to a deeper understanding of the impact of [6]-Gingerol on plasma membrane properties.

Resumen

El análisis de la interacción de xenobióticos, agentes farmacéuticos, nanopartículas, y otros compuestos con las membranas celulares plantea numerosos desafíos, mayormente debidos a la complejidad estructural y funcional de las membranas celulares. Con el fin de superar estas limitaciones, en la investigación elemental de dichas membranas se hace uso de modelos de membrana artificiales, que permiten control preciso en su composición y propiedades. En este trabajo de fin de Máster, se utiliza la técnica de Langmuir para modelar la membrana plasmática sana y enferma de colonocitos en pacientes con enfermedades intestinales inflamatorias (IBD), en la interfase aire-agua. Estos modelos de membrana son utilizados para investigar su interacción con [6]-Gingerol, un xenobiótico conocido por sus propiedades antioxidantes, antiinflamatorias, y antitumorales, así como de su función protectora en pacientes con IBD. Sin embrago, la baja solubilidad en agua del [6]-Gingerol restringe severamente su biodisponibilidad, y por tanto su uso como agente terapéutico. El objetivo de este trabajo de fin de Máster es la obtención de información sobre las interacciones moleculares presentes entre [6]-Gingerol y los componentes de membranas plasmáticas, ofreciendo la posibilidad de sentar las bases para el futuro desarrollo de sistemas de distribución (como liposomas o exosomas artificiales) con el fin de mejorar el potencial terapéutico del [6]-Gingerol. El efecto de [6]-Gingerol en la fluidez de membrana, así como de estabilidad, y propiedades termodinámicas fue estudiado a partir de los datos extraídos de las isotermas de presión superficial-área por molécula. Los resultados obtenidos indican un aumento en la fluidez de las membranas al aumentar χ_{GIN}. Desde un punto de vista termodinámico, ambos modelos de membrana muestran interacciones repulsivas con [6]-Gingerol, siendo estas generalmente más fuertes en el caso de la membrana sana. La incorporación de [6]-Gingerol en ambos modelos de membrana se llevó a cabo mediante experimentos de adsorción, en los que se analizaron las medidas registradas de presión superficial. Adicionalmente, este proceso se visualizó *in situ* mediante microscopía de ángulo de Brewster (BAM). En conclusión, el [6]-Gingerol es capaz de incorporarse en ambos modelos de membrana, exhibiendo una incorporación más favorecida en la membrana sana. Todos estos hallazgos resaltan el distinto comportamiento termodinámico y estructural de los modelos de membrana sana y afectada por IBD, bajo la influencia de [6]-Gingerol, contribuyendo a una mejor comprensión del impacto de [6]-Gingerol en las propiedades de las membranas plasmáticas.

1. Objectives

This Final Master's Thesis has essentially an academic nature aimed at consolidating the multidisciplinary knowledge and skills achieved at a Master's level. Some of the skills to be acquired in this project include the responsible and autonomous work in the laboratory, as well as the critical and scientific thinking, problem-solving capabilities, bibliographic research, and the communication of results both in written and oral expositions.

In addition, this thesis develops a research project in the laboratory and thus presents scientific-related objectives. From a scientific point of view, this project aims at the development of model cell membranes (healthy and disturbed) using the Langmuir technique and the subsequent study of the molecular interactions of these model cell membranes with [6]-Gingerol through the analysis of thermodynamic properties. Consequently, this thesis provides knowledge in nanoscale modelling techniques, molecular interaction studies using thermodynamic analysis, and the characterization of model cell membranes as well as their interactions with [6]-Gingerol using techniques at the air-water interface, such as Brewster Angle Microscopy (BAM).

2. Introduction

Plasma membranes are essential structures in biological systems, serving as flexible barriers that preserve cellular integrity and mediate molecular transport. They are selectively permeable to polar molecules, making them critical for various cellular phenomena. The main components of plasma membranes are phospholipids, proteins, carbohydrates, and cholesterol. Their structure consists of a lipid bilayer where, due to the amphipathic nature of lipids, the hydrophilic heads of lipids face outward, whereas the hydrophobic chains remain inside.[1]

A study conducted in the United States in 2006 revealed that over 60% of the commercialized drugs target multiple plasma membrane components.[2] For this reason, understanding the different mechanisms of interaction between plasma membranes with other molecules of interest, such as proteins or drugs, is crucial for the development of novel drugs and therapies. Additional information can be obtained, such as virus effects and cytotoxicity in plasma membranes.[3]

Due to the complexity of cell membranes, their extraction and research by direct methods presents significant challenges. Thereby, the use of artificial cell membranes that mimic the behavior of those in living organisms is prevalent in the literature. Various cell membrane models are typically used.[4] Among them, Langmuir monolayers, Langmuir-Blodgett (LB) films and Langmuir-Schaefer (LS) films offer excellent control over the packaging of selected molecules within model cell membranes, allowing precise definition of the molecular density by varying the area per molecule by means of a Langmuir trough.[5–8]

In this Final Master's thesis, the Langmuir technique is used to model intestinal epithelium cells (IECs). IECs, along with mucus, are the main components of the intestinal mucosal barrier, which separates the body from the luminal contents of the gut, allowing nutrient absorption, and waste secretion while offering protection against pathogens or toxic agents. The intestinal epithelium is comprised of a monolayer of highly specialized cells, including absorptive enterocytes (called colonocytes when referring to the colon, corresponding to the most abundant IECs), goblet cells, and Paneth cells, among others.[9–11] Enterocytes are not only responsible for nutrient absorption but they also play a crucial role in monitoring gut homeostasis, and thus fulfilling a critical protective function against pathogens.[11] Given the importance of these IECs, this Master's thesis focuses on modelling their plasma membrane to shed light on the mechanisms of action of a well-known beneficial xenobiotic in intestinal bowel disease (IBD): [6]-Gingerol.

IBDs are chronic inflammatory disorders affecting the gastrointestinal tract and increasing the risk of colitis-associated cancer.[12] The pathogenesis of IBD is complex, as there are multiple factors promoting IBD in an individual (genetic, environmental, and immunologic factors). The two main types of IBD are Crohn's disease (CD) and ulcerative colitis (UC). One key difference between these conditions is the affected intestinal area: CD affects both the small intestine and the colon, whereas UC affects the colon exclusively.[13] In a population-based study on Crohn's disease in Europe, 27% of interviewees were found to have exclusive involvement of the small intestine, while 73% of Crohn patients had involvement in the colon (either being only colitis or affecting both the ileum and the colon).[14] It is for this reason that the IECs selected for modelling in this Master's thesis were colonocytes.

To date, there are no curative treatments for IBD. Current therapies, including aminosalicylates, antibiotics, steroids, and immunomodulators, are used to reduce inflammation and to minimize symptoms to bring patients into stable remission.[13] However, most of these therapeutic strategies are inconsistent for IBD patients and may cause severe side effects, such as renal toxicity and hepatoxicity.[15] For these reasons, novel drugs and therapies are needed to effectively treat IBD.

A key feature reported in IBD is the increase in the intestinal permeability, as well as the alteration of lipid metabolism.[16–18] The loss of the mucus layer integrity is one of the primary factors contributing to the disruption of intestinal permeability.[19] Importantly, there have been reports of changes in the lipid composition and fluidity of cell membranes, including those of erythrocytes and mucosal cells.[20,21]

In this Master's thesis, colonocytes are modelled using six lipids: cholesterol (CHOL), dipalmitoylphosphatidylcholine (DPPC), phosphatidylethanolamine (PE), phosphatidylserine (PS), phosphatidylinositol (PI), and sphingomyelin (SM). Their corresponding chemical structures are shown in Figure 1. Both a 'healthy' colonocyte as well as an 'IBD-affected' colonocyte are modelled in this project. These model cell membranes are subsequently exposed to [6]-Gingerol (GIN), a xenobiotic found in ginger.

Ginger (*Zingiber officinale Roscoe*) is a plant from the Zingiberaceae family that has been used as a dietary spice and for the treatment of various diseases in China and India for over 5000 years.[22] Ginger has been widely studied due to its reported anti-inflammatory, antioxidant and antitumoral properties.[22–29] Importantly, ginger has also been used in the treatment of IBD.[30] A major challenge associated with the active components of ginger is their rather low solubility in water, which results in low bioavailability. One notable study[31] reported the findings of *in vitro* and *in vivo* investigations into the therapeutic effects of ginger-derived nanoparticles (NPs) for the treatment of IBD. The extracted conclusions are promising: the synthesized ginger-derived NPs were found to both promote intestinal mucosal healing and to serve as a preventive tool against colitis. The curative properties of these NPs were attributed to the anti-inflammatory effects of ginger. Nonetheless, the use of NPs presents a major drawback, which lies in their potential toxicity. More specific formulations targeting ginger bioactive molecules, such as liposomes or artificial exosomes, could prove more

effective in reducing the side effects associated with NPs or other drugs, thanks to their enhanced biocompatibility.

To simplify the study, better understand the mechanisms of action of ginger in IBD, and more importantly develop advanced formulations of ginger-related drugs, [6]-Gingerol has been the focus of investigation in this thesis. The reason behind this choice is that, among the 14 identified bioactive compounds in fresh ginger,[22] gingerols are the major components, with [6]-Gingerol being the most abundant.[32] [6]-Gingerol is a beta-hydroxy ketone that contains a vanillyl group, as illustrated in Figure 1 . It has a length of approximately 1.8 nm, it is neutrally charged, and it contains two hydrogen-bond donor atoms and four hydrogen-bond acceptor atoms, enabling intermolecular interactions. The high number of rotatable bonds (ten bonds) provides the molecule with a high conformational flexibility.

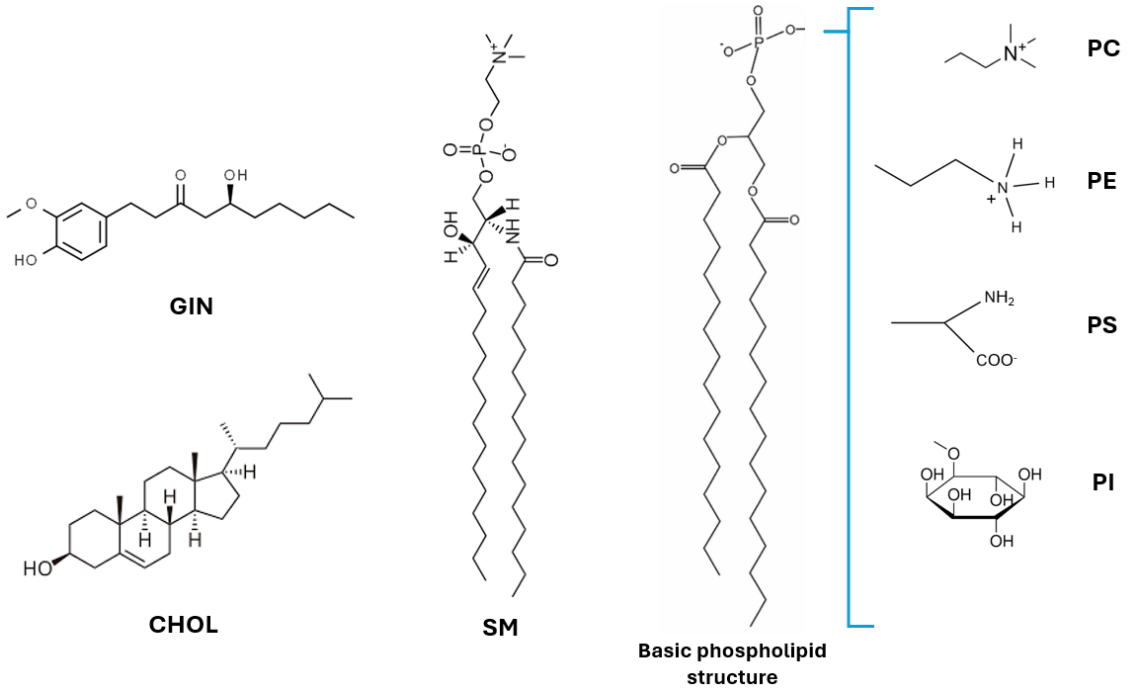

Figure 1. Chemical structure of [6]-Gingerol (GIN), cholesterol (CHOL), sphingomyelin (SM), phosphatidylcholine (PC), phosphatidylethanolamine (PE), phosphatidylserine (PS), phosphatidylinositol (PI). Refer to the Experimental Section (**3.1**) for the specific chain insaturations of PC, PE, PS, and PI used in this project.

Despite the promising potential of [6]-Gingerol and its well-known bioavailability challenges, there is a notably lack of research on the encapsulation of [6]-Gingerol in vesicles and other delivery methodologies, with only a few reports in the field.[33–35] To address this gap, our research group has focused on investigating the surface properties

of [6]-Gingerol and its interactions with selected components of cell membranes, which was the core subject of my Final Degree Project (TFG).[36,37] In this Final Master's Thesis that work is extended with the primary objective of deepening our understanding of how [6]-Gingerol interacts with 'healthy' and 'IBD-affected' model cell membranes, establishing a groundwork for more ambitious future research in the development of innovative delivery systems that could significantly enhance the bioavailability of this compound, thereby unlocking its therapeutic potential for the treatment of diseases, such as IBD.

3. Experimental section

3.1 Materials

10 mg of [6]-Gingerol (GIN, ≥ 98%, Sigma-Aldrich) were dissolved in chloroform to prepare a stock solution at a concentration of $6.26 \cdot 10^{-4}$ M. The stock solution was sonicated for 5 minutes to prepare diluted [6]-Gingerol solutions at a concentration of 10^{-5} M. Prior to use, [6]-Gingerol solutions underwent ultrasonic processing for 3 minutes to prevent molecular aggregation. Appropriate amounts of cholesterol (CHOL, ≥ 99%, Sigma-Aldrich), 1,2-dipalmitoyl-sn-glycero-3-phosphocholine (DPPC, ≥ 99%, Sigma-Aldrich), 1,2-diheptadecanoyl-*sn*-glycero-3-phospho-L-serine (sodium salt) (PS, >99%, Avanti), 1,2-Diacyl-*sn*-glycero-3-phosphoethanolamine (PE, USP Reference Standard, USP/Sigma-Aldrich), L-α-Phosphatidylinositol sodium salt (PI, ≥ 98% Sigma-Aldrich), and N-Palmitoyl-D-sphingomyelin (SM, ≥ 99%, Sigma-Aldrich) were used to prepare 10^{-4} M solutions in chloroform (PS and PI solutions were prepared in chloroform:ethanol in a 9:1 ratio). All solutions were stored in a freezer to prevent degradation. Chloroform was purchased from Macron Fine Chemicals (≥99.8%, CAS 67-66-3). Ethanol was purchased from Laboaragón (≥99.5%, CAS-64-17-5). The appropriate volumes of the stock solutions were used to prepare the respective binary (GIN-CHOL, GIN-DPPC, GIN-PE, GIN-PS, GIN-PI, and GIN-SM) mixtures, as well as the 'healthy' (HM) and 'IBD-affected' (DM) model membranes.

The troughs were cleaned using acetone (≥99.5%, Sigma-Aldrich CAS 67-64-1), chloroform, and Milli Pore Milli-Q water from the INMA purification system (resistivity 18.2 MΩ·cm). The trough barriers were cleaned using acetone and Milli-Q water. The subphase used in all experiments was Milli Pore Milli-Q water.

3.2 Methods

3.2.1 The Langmuir technique

The Langmuir technique allows the preparation of well-ordered monolayers of amphiphilic compounds at the air-water interface. The experiment is done using a trough with a depth of a few millimetres, filled with a solvent (commonly water) designated as the subphase. Two mobile barriers are positioned on the sides of the trough, while a Wilhelmy balance is positioned in the middle of the trough. The Wilhelmy balance measures surface pressure, π (defined by Equation 1), upon the compression process.

$$\pi = \gamma_0 - \gamma \tag{1}$$

where γ_0 is the surface tension of the clean subphase (water in our case), and γ is the surface tension of the subphase covered by the Langmuir film.

By means of a Hamilton micro-syringe, the molecules of interest are spread onto the water surface. The solvent used in the spreading solutions must be volatile, insoluble in the subphase, and have a positive dispersion coefficient, S, relative to the liquid in the subphase, ensuring spontaneous dispersion over the surface. Once the molecules are spread and the volatile solvent evaporated (ca. 15 min after the last drop is spread), the compression process begins, driven by the movement of the mobile barriers. The compression of the monolayer, with the simultaneous recording of the surface pressure and the area per molecule, takes place at constant temperature.

When plotting surface pressure versus area per molecule, a compression isotherm (π-A) is obtained. This isotherm is unique and characteristic to each molecule and provides information about the different phases and phase transitions the molecules undergo upon compression, as illustrated in Figure 2.

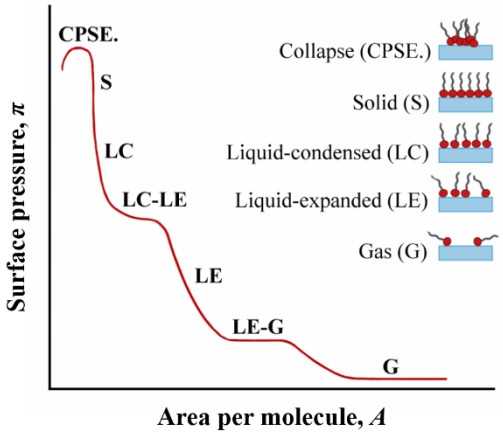

Figure 2. Generic π-A isotherm showing the different monolayer phases upon compression.

At the beginning of the compression process, the molecules are widely scattered, resulting in minimal intermolecular interactions, and the recorded surface pressure values are very low (the monolayer is in the so called gas phase, G). As the area per molecule decreases, the

monolayer transitions into progressively more ordered phases, leading to a rise in surface pressure. These phases may include the liquid expanded (LE) phase, coexistence of liquid expanded and liquid condensed (LC) phases (LE-LC), LC, and finally the solid (S) phase. Each monolayer eventually reaches a collapse surface pressure, where the molecules stack upon one another. It is worth noting that not all phases are observed in every case, as this depends on the nature of the monolayer, and the specific experimental conditions (mainly the temperature).

In this Master's thesis, π-A isotherms were recorded in a Teflon® trough with polyoxymethylene barriers, placed within an enclosed compartment in a semi-clean room (Appendix A). The initial area per molecule for each registered isotherm was set to 2.15 $nm^2 \cdot molecule^{-1}$, and the temperature for every experiment was 20 ± 1 ºC. To ensure proper experimental conditions, a rigorous cleaning protocol was followed: the trough and barriers were thoroughly cleaned using acetone and chloroform, allowing the solvents to evaporate for 15 minutes. Subsequently, cleanliness of the water surface was verified by performing a blank experiment prior to each measurement. Once confirmed, the desired molecules were carefully spread onto the water surface using a Hamilton micro-syringe. After allowing the spreading solvent to evaporate for 15 minutes, the compression process slowly began at a compression rate of 10 $mm \cdot min^{-1}$.

3.2.2 Mixtures and thermodynamic analysis

The data obtained from the π-A isotherms were used to calculate multiple thermodynamic parameters, providing insights into the miscibility, stability, and fluidity of the resulting mixed monolayers. One of the parameters analysed in this work is the excess area of mixing, A^E, which is defined as follows: [38]

$$A^E = A_{mix} - A_{ideal} = A_{mix} - \sum_i \chi_i A_i \qquad (2)$$

where A_{mix} ($nm^2 \cdot molecule^{-1}$) represents the experimental area per molecule at the studied surface pressure, π ($mN \cdot m^{-1}$); χ_i is the molar fraction of each studied component, *i*, and A_i denotes the area per molecule ($nm^2 \cdot molecule^{-1}$) of the single components at the designated surface pressure value. The excess area provides valuable insights into the miscibility of the components in a mixture and the nature of intermolecular interactions between the components (attractive or repulsive). When $A^E = 0$, the components in the mixture are considered ideally miscible or completely immiscible. In contrast, $A^E \neq 0$

indicates partial miscibility. $A^E < 0$ values suggest the presence of attractive intermolecular interactions and/or more efficient molecular packing, due to steric factors. Finally, $A^E > 0$ values are indicative of repulsive interactions and/or a less effective molecular packing.

Another relevant thermodynamic property that can be derived from π-A isotherms is the Gibbs excess energy of mixing, ΔG_m^E.[39–41]

$$\Delta G_m^E = \int_0^\pi A_{mix}\, d\pi - \sum_i \chi_i \int_0^\pi A_i\, d\pi \quad (3)$$

$\Delta G_m^E < 0$ values are indicative of strong attractive interactions between the monolayer components, suggesting favourable mixing. In contrast, $\Delta G_m^E > 0$ values indicate repulsive interactions, deviating from ideal behaviour.

To evaluate the stability of the obtained monolayers, the Gibbs energy of mixing, ΔG_m, was also calculated in this study, as following:[41]

$$\Delta G_m = \Delta G_m^E + \Delta G_m^{ideal} = \Delta G_m^E + RT \sum_i \chi_i \ln \chi_i \quad (4)$$

where *R* is the constant for ideal gases, and *T* the experiment temperature. $\Delta G_m < 0$ values are indicative of a stable monolayer, while $\Delta G_m > 0$ values are characteristic of unstable monolayers.

Finally, the 2D compression modulus, Ks, (inverse of the compressibility coefficient, Cs) was calculated to obtain information about the fluidity of the monolayers at the air-water interface. Ks values were calculated as following:[42]

$$K_s = C_s^{-1} = -A\left(\frac{d\pi}{dA}\right)_T \quad (5)$$

Accordingly to the classification by Davies and Rideal, the G phase is characterized by Ks values ranging from 0 to 12.5 $mN \cdot m^{-1}$; Ks values in the 12.5-50 $mN \cdot m^{-1}$ range indicate a LE phase; regions where Ks values are between 50 and 100 $mN \cdot m^{-1}$ are indicative of a LE-LC transition phase; Ks values between 100 and 250 $mN \cdot m^{-1}$ correspond to the LC phase, and values exceeding 1000 $mN \cdot m^{-1}$ are associated with the S phase.[42]

3.2.3 [6]-Gingerol adsorption experiments

The subsequent step in this project, was to study the ability of GIN to adsorb into the membranes, simulating its absorption from the bloodstream into the intestinal epithelium. This step aims to explore from a physicochemical point of view the potential therapeutic application of GIN for patients with IBD. The methodology followed was to first prepare the model membrane at the air-water interface, allowing it to stabilize until a biological surface pressure[43] of ~30 $mN \cdot m^{-1}$ was reached. Subsequently, a GIN solution in ethanol was injected in the water subphase while monitoring the surface pressure as a function of time. An increase in the surface pressure following injection would indicate the adsorption of molecules into the monolayer, while a decrease in the surface pressure would suggest that the molecules in the membrane are being drawn into the subphase by GIN and/or ethanol molecules. Low contents of GIN were used in these experiments (χ_{GIN}=0.1-0.3, relative to the model membrane). Given GIN is very insoluble in water, it was anticipated that most of GIN would float to the water surface. Since ethanol has a smaller density than water, when it is injected in the water subphase it is prone to resurface, thus blank controls were carried out injecting ethanol to determine the magnitude of its influence in the obtained results.

These experiments were carried out using two different setups, each with its own pros and cons. The first setup consists of a mini-trough (KSV Minimicro, 167 x 50 mm^2) comprising a small open hole on one side, allowing the injection of solutions into the subphase without disturbing the monolayer at the air-water interface. A potential drawback of this methodology is that the injected solution may diffuse throughout all the subphase and resurface in areas that are not covered by the model membrane. This issue is avoided in the second setup, in which a 5 mm diameter glass beaker-like is used to prepare the model cell membranes by spreading the molecules till the target surface pressure is reached. The main drawback here is that the organization of the lipids in the membrane may be not as good as in the Langmuir trough. Importantly, although this approach is more invasive (requiring the syringe containing the GIN solution to be inserted vertically, potentially disturbing the monolayer) it offers the advantage of minimizing diffusion effects of the injected solution. Consequently, the experiments conducted using this method served to quantify the diffusion effects observed with the first setup, providing a basis for comparison.

The first step was to determine the time needed for the surface pressure of each monolayer to stabilize. This was done by forming the monolayer of each system at a target surface pressure of 35 $mN \cdot m^{-1}$ (in order to have a biological surface pressure of around 30 $mN \cdot m^{-1}$ at the time of injection) and measuring surface pressure vs time. As shown in Figure 3, both systems needed approximately 2 hours for each monolayer to stabilize. Then, adsorption experiments were performed.

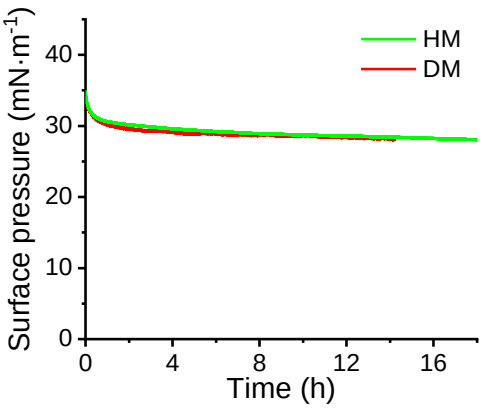

Figure 3. Surface pressure vs time for the healthy membrane (HM) and the diseased membrane (DM) monolayers recorded at 21 ºC.

3.2.4 Brewster Angle Microscopy (BAM)

Brewster Angle Microscopy (BAM) is a powerful characterization tool that provides direct visualization of monolayers at the air-water interface. The working principle of this technique is the following: when a p-polarized light beam is directed at the pure air-water interface at the Brewster angle, α (α=53º for an air-water interface) no reflection occurs, i.e., all the light is transmitted through the water subphase. A light trap is placed beneath the laser beam in the subphase; if there is no monolayer at the air-water interface, no light is detected, and the resulting image appears black. If there is a monolayer at the air-water interface, the light (if the incident angle α=53º is maintained) is reflected due to the change in the refraction index at the interface. The reflected light is then detected by a camera, producing a 2D black and white image. The brightness of the image is proportional to the surface density and the tilt angle of the molecules. Domains with different tilt angles appear as regions with varying contrast.[44,45]

BAM was used to visualize the model membranes at different surface pressure values, as well as to study the adsorption of GIN molecules into the modelled membranes. In these last experiments, a glass Petri-dish was used. Molecules forming the model membrane were spread onto the subphase until the desired target surface pressure was achieved. Subsequently, GIN was injected in the subphase. The setup used for the BAM experiments is shown in Appendix B.

4. Results and discussion

4.1 Single monolayers

A preliminary study of the monolayers for each lipid in the model membrane, along with [6]-Gingerol, was conducted using the Langmuir technique. The corresponding π-A isotherms were recorded (Figure 4, left panel). The data was used to generate Ks-π plots, which were analysed to identify the different phases of each monolayer upon the compression process, as shown in Figure 4, right panel. Table 1 compiles the main features of the π-A isotherms and Ks-π plots of these compounds.

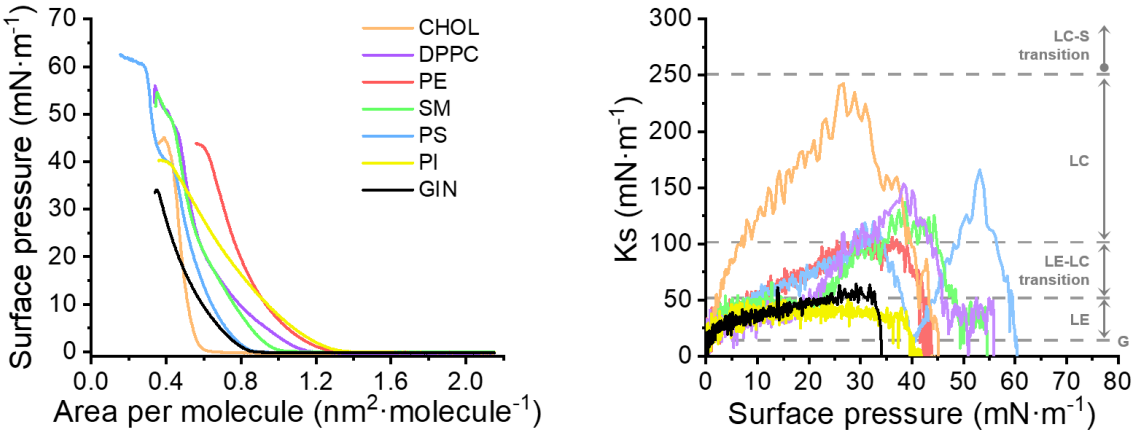

Figure 4. Left panel: π-A isotherms for CHOL, DPPC, PE, SM, PS, PI, and GIN monolayers registered at 20±1 ºC. **Right panel:** Ks-π plots for CHOL, DPPC, PE, SM, PS, PI, and GIN monolayers.

The π-A isotherm for the GIN monolayer shows the lift-off of at ca. 0.86 $nm^2 \cdot molecule^{-1}$ and the collapse at ca. 0.35 $nm^2 \cdot molecule^{-1}$, with a surface pressure of 34.0 $mN \cdot m^{-1}$. In the Ks-π plot, the monolayer transitions from a G to an LE phase at a surface pressure of 0.2 $mN \cdot m^{-1}$, reaching a LE-LC transition phase at 19.5 $mN \cdot m^{-1}$. The maximum value of Ks (corresponding to highest monolayer stability) observed is 64.3 $mN \cdot m^{-1}$, corresponding to a surface pressure of 29.2 $mN \cdot m^{-1}$. The fluidity of a GIN monolayer is tentatively attributed here to its chemical structure: GIN molecules contain two hydrogen-bond donor atoms, four hydrogen-bond acceptor atoms, which allow intermolecular interactions between other GIN molecules as well as water molecules from the subphase. Additionally, the presence of a high number of rotatable bonds (ten) grants the molecule with high conformational flexibility.

The high compression modulus of the CHOL monolayer can be attributed to its planar

molecular structure, resulting from the trans conformation in which molecules arrange, which allows for intermolecular π-π stacking and hydrogen bonding with other CHOL molecules or water molecules via the -OH group. In contrast, the other lipids present more fluid monolayers, mainly attributable to their long aliphatic chains, which provide high conformational flexibility. As for the PS monolayer, the plateau in its π-A isotherm, corresponding to a visible phase transition, has been previously reported in the literature;[46] it has been related to the experimental conditions, especially to temperature and humidity.[47]

Table 1. Compilation of the data extracted from π-A isotherms and respective Ks-π plots of the prepared single monolayers.

Monolayer	CHOL	DPPC	PE	PS	PI	SM	GIN
$A_{LIFT-OFF}$ ($nm^2 \cdot molecule^{-1}$)	0.61	1.15	1.56	0.87	1.30	1.00	0.86
$\pi_{G \rightarrow LE}$ ($mN \cdot m^{-1}$)	0.3	0.4	0.4	0.2	0.1	0.2	0.2
$\pi_{LE \rightarrow LC}$ ($mN \cdot m^{-1}$)	2.5	20.3	7.8	7.9	-	5.2	19.5
$\pi_{LC \rightarrow S}$ ($mN \cdot m^{-1}$)	6.2	26.4	25.4	28.3	-	33.0	-
$A_{COLLAPSE}$ ($nm^2 \cdot molecule^{-1}$)	0.39	0.34	0.59	0.27	0.40	0.35	0.35
$\pi_{COLLAPSE}$ ($mN \cdot m^{-1}$)	45.1	56.0	43.3	60.9	40.0	54.6	34.0
Maximum Ks ($mN \cdot m^{-1}$)	242.8	153.6	107.9	166.0	38.0	137.0	64.3
$\pi_{maximum\ Ks}$ ($mN \cdot m^{-1}$)	26.7	38.4	29.5	53.1	5.5	38.6	29.2

In summary, the monolayers can be ordered from most to least ordered according to the most condensed phase reached: CHOL>PS>DPPC>SM>PE>PI>GIN. At a surface pressure of 30 $mN \cdot m^{-1}$, which corresponds to the biological surface pressure in eukaryotic cells[43], the order is the following: CHOL>PS=DPPC>PE>SM>GIN>PI. CHOL presents the most ordered monolayers, while PI the least ordered ones, i.e., the most fluid monolayers. GIN also results in very fluid monolayers.

4.2 Binary monolayers

The isotherms for binary monolayers of GIN with each lipid were obtained at three different molar fractions of GIN (χ_{GIN}= 0.3, 0.5 and 0.7) to better understand how GIN interacts with each component of the later-on-discussed model membranes.

The fluidity of the binary monolayers was analysed through Ks-π plots (Appendix C). A general trend emerges: the higher the GIN content in a lipid monolayer, the greater the fluidity of the binary monolayer. The fluidizing effect of GIN is stronger depending on the nature of the opposite pure component: with CHOL, PE, SM and PS monolayers, maximum fluidity occurs at χ_{GIN}=0.7; for DPPC, a low GIN content (χ_{GIN}=0.3) is enough to maximize the fluidity up to a surface pressure of ca. 30 $mN \cdot m^{-1}$. For PI, since its monolayer already exhibits similar fluidity to a GIN monolayer, adding GIN does not significantly alter its fluidity.

To obtain information about the miscibility and stability of the binary mixtures, Equations 2,3 and 4 (**3.2.2 section**) were applied to these binary systems. The target surface pressure values for this thermodynamic study were 5, 10, 15, 20, 30 and 33 $mN \cdot m^{-1}$.

Figure 5 illustrates A^E values for the binary mixtures. Most show slightly positive A^E values, indicating repulsive interactions between GIN and each membrane component. In GIN-DPPC, GIN-PE, and GIN-PS mixtures, A^E decreases with increasing surface pressure. In contrast, for GIN-CHOL, GIN-SM, GIN-PI mixtures, A^E increases with surface pressure, reflecting stronger the repulsive forces at higher pressures. Some exceptions to the above observations include GIN-CHOL (χ_{GIN}=0.5) and GIN-SM (χ_{GIN}=0.5;0.7), which exhibit slightly negative A^E values, indicating attractive forces between the components. The most miscible mixture is GIN-CHOL (χ_{GIN}=0.5) at 15 $mN \cdot m^{-1}$, with A^E = -0.034 $nm^2 \cdot molecule^{-1}$, while the least miscible mixture is GIN- PS (χ_{GIN}=0.3) at 5 $mN \cdot m^{-1}$, with A^E = 0.085 $nm^2 \cdot molecule^{-1}$. At the biologically relevant surface pressure of 30 $mN \cdot m^{-1}$, the most miscible mixtures are GIN-CHOL (χ_{GIN}=0.5, A^E = -0.026 $nm^2 \cdot molecule^{-1}$) and GIN-SM (χ_{GIN}=0.7, A^E = -0.023 $nm^2 \cdot molecule^{-1}$).

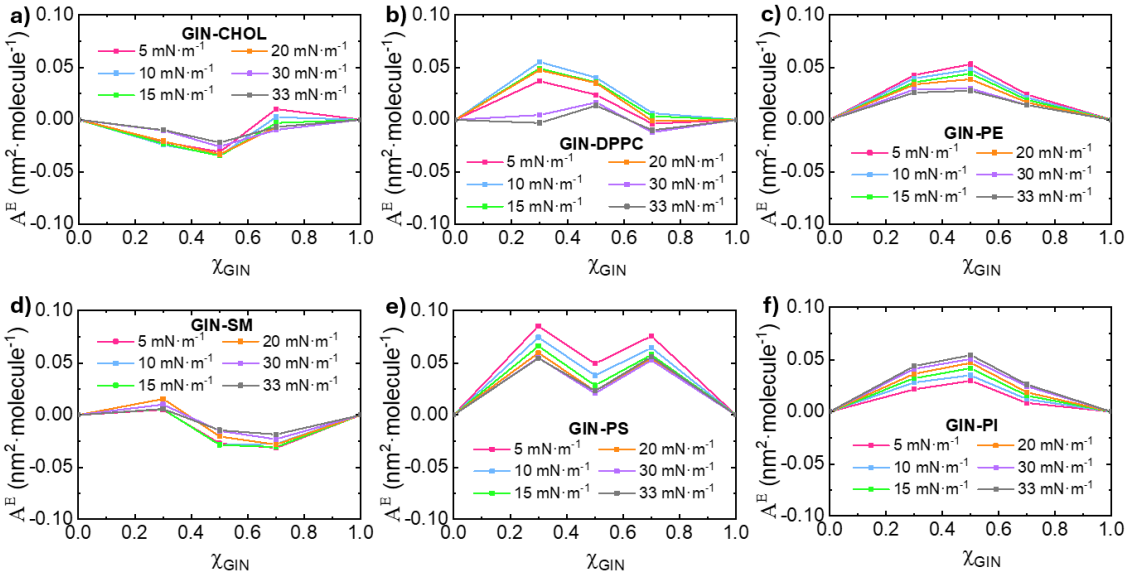

Figure 5. Excess area of mixing vs. GIN molar fraction for the a) GIN-CHOL, b) GIN-DPPC, c) GIN-PE, d) GIN-SM, e) GIN-PS, and f) GIN-PI binary systems.

To further assess the stability of the binary mixtures, ΔG_m^E was determined, whilst the stability of the mixtures was evaluated from the ΔG_m values. Figure 6 shows the calculated ΔG_m^E values for all mixtures. Following a similar trend as before, most of mixtures exhibit ΔG_m^E positive values, indicating poor miscibility. For GIN-DPPC, GIN-PE, GIN-PS and GIN-PI mixtures, ΔG_m^E increases with surface pressure, indicating more repulsive interactions. In the case of GIN-CHOL and GIN-SM mixtures, ΔG_m^E decreases with surface pressure, revealing stronger attractive interactions as surface pressure increases. The most thermodynamically favourable mixtures are the ones with the lowest ΔG_m^E values, which correspond to GIN-CHOL (χ_{GIN}=0.5 at 30 mN·m^{-1} with ΔG_m^E= -644 J·mol^{-1}), and GIN-SM (χ_{GIN}=0.7 at 30 mN·m^{-1}, with ΔG_m^E= -535 J·mol^{-1}, and at 33 mN·m^{-1}, with ΔG_m^E= -535 J·mol^{-1}). The least stable mixtures, i.e., the mixtures with the highest ΔG_m^E values are GIN-PS (χ_{GIN}=0.3 at 33 mN·m^{-1}, with ΔG_m^E= -1400 J·mol^{-1}) and GIN-PS (χ_{GIN}=0.7 at 33 mN·m^{-1}, with ΔG_m^E= -1191 J·mol^{-1}). At a surface pressure of 30 mN·m^{-1}, the most stable mixtures are GIN-CHOL (χ_{GIN}=0.5 at 30 mN·m^{-1}, ΔG_m^E= -644 J·mol^{-1}), and GIN-SM (χ_{GIN}=0.7 at 30 mN·m^{-1}, ΔG_m^E= -535 J·mol^{-1}). In contrast, the GIN- PS system exhibits ΔG_m^E values exceeding 1200 J·mol^{-1}, previously linked to phase separation between components in model cell membranes.[48] This finding is also consistent with the presence of two maxima in both A^E and ΔG_m^E plots, which is also associated to phase segregation phenomena.[49]

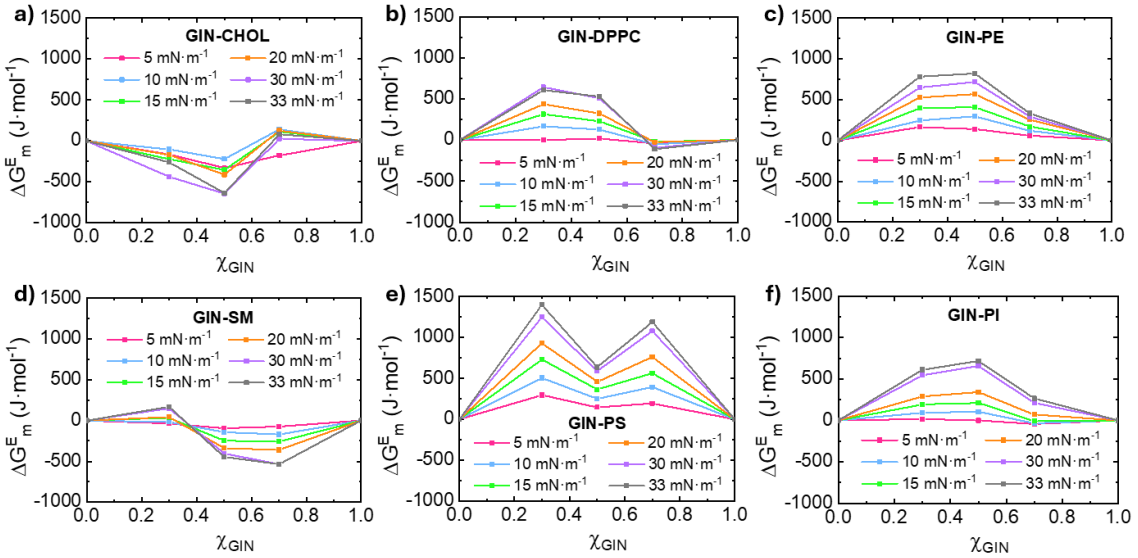

Figure 6. Excess Gibbs energy of mixing vs. GIN molar fraction for the a) GIN-CHOL, b) GIN-DPPC, c) GIN-PE, d) GIN-SM, e) GIN-PS, and f) GIN-PI binary systems.

Figure 7 presents the ΔG_m values for the here studied binary mixtures. All mixtures exhibit negative ΔG_m values, indicating thermodynamic stability. For most of mixtures, ΔG_m increases with surface pressure, except for GIN-CHOL, and GIN-SM, where it decreases. The most stable systems, with the lowest ΔG_m values, are GIN-CHOL (χ_{GIN}=0.5 at 30 mN·m^{-1} with ΔG_m= -2344 J·mol^{-1} and at 33 mN·m^{-1} with ΔG_m= -2338 J·mol^{-1}), and GIN-SM (χ_{GIN}=0.5 , ΔG_m= -2145 J·mol^{-1} at 33 mN·m^{-1}). The least stable binary mixtures are GIN-PS (χ_{GIN}=0.3 at 33 mN·m^{-1}, ΔG_m= -98 J·mol^{-1}) and GIN-PS at (χ_{GIN}=0.7, ΔG_m= -307 J·mol^{-1} at 33 mN·m^{-1}). The most stable mixtures at the biologically relevant surface pressure of 30 mN·m^{-1} are GIN-CHOL (χ_{GIN}=0.5, ΔG_m= -2344 J·mol^{-1}) and GIN-SM (χ_{GIN}=0.5, ΔG_m= -2103 J·mol^{-1}).

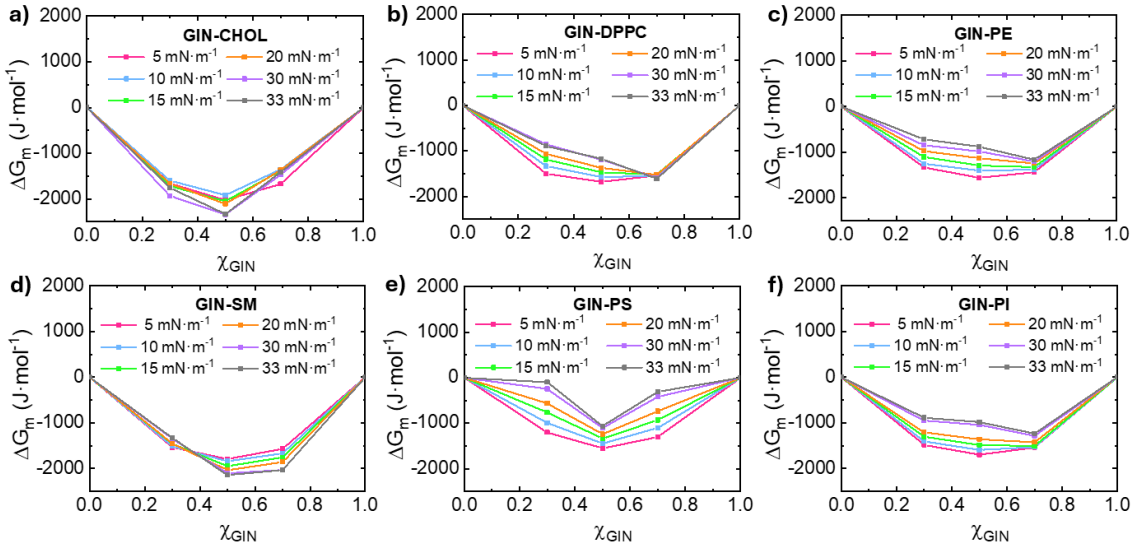

Figure 7. Gibbs energy of mixing vs. GIN molar fraction for the a) GIN-CHOL, b) GIN-DPPC, c) GIN-PE, d) GIN-SM, e) GIN-PS, and f) GIN-PI binary systems.

In conclusion, taking together all these results, the most favourable binary mixture from a thermodynamic point of view at a biological surface pressure (30 $mN \cdot m^{-1}$) is GIN-CHOL at χ_{GIN}=0.5 (A^E = -0.026 $nm^2 \cdot molecule^{-1}$, ΔG_m^E= -643.5 $J \cdot mol^{-1}$, ΔG_m= -2343.6 $J \cdot mol^{-1}$).

4.3 Model membranes

4.3.1 Composition of model membranes

The composition of the modelled healthy membrane (HM) here used was determined based on the lipidome analysis of a commercial human colon cell line.[50] Alkenyl phosphatidylethanolamine was included in the total phosphatidylethanolamine percentage, as both belong to the same lipid family. The cholesterol to phospholipid ratio was set at 1:1, consistent with the typical ratio found in mammalian cells, 1:1.[51,52]

The composition of the outer layer of the HM, was determined considering the asymmetric distribution of phospholipids in intestinal cell membranes.[53] Whilst the distribution of cholesterol within the bilayer remains a topic of debate, current evidence suggests an asymmetric distribution rather than an even one.[54] In this work, cholesterol distribution was estimated taking into account the conclusions of extensive coarse-grained molecular dynamics simulation studies[55], which revealed that the distribution of cholesterol in the membrane depends on the lipid composition of both leaflets. Specifically, cholesterol prefers surrounding itself by anionic lipids over neutral ones, and prefers saturated acyl chains over unsaturated chains (being this effect weaker than the

previous statement). The HM bilayer contains two anionic lipids, PS and PI, both of which, like DPPC, contain saturated chains. These anionic lipids are mainly located in the inner leaflet, leading to an estimated cholesterol distribution in the inner leaflet in a 60-40 % ratio. Taking together all these factors, the composition of the outer layer of HM was established, as shown in Figure 8.

As for the 'IBD-affected' model membrane (diseased membrane, DM), a literature review was performed to examine the lipid changes associated with IBD, including Crohn's disease and ulcerative colitis. Overall, results were highly controversial due to the variability in sample types and experimental procedures. Ultimately, lipid level alterations reflected in this thesis' DM were based on an experimental colitis study[21], which was chosen because it was the only study that confirmed that the analysis was limited to intestinal epithelial cells, unlike other studies that included additional mucosal cells. This study evaluated the variations in the ratios of DPPC, CHOL, SM and PE, finding that DPPC remains constant, while the ratios of the other lipids decrease in patients with colitis. These findings were used to define our DM model, where the magnitude of each variation was multiplied by a factor of 100 to facilitate a more robust comparison of the effects of GIN between the HM and DM models. PS is a lipid predominantly found in the inner leaflet in a healthy membrane. However, PS translocates to the outer leaflet, where it serves as an apoptotic signal for macrophages to "eat".[56] In IBD, apoptosis has been reported to occur in the intestinal epithelium.[57] For applicability purposes, a non-apoptotic scenario was assumed, meaning that PS levels remain constant in both leaflets. As for PI, no information about its alteration in colonic cells was found, therefore its levels were also considered to remain unaffected in the DM model. Based on these lipid variations, the CHOL to phospholipid ratio was maintained at 1:1. Figure 8 shows the DM composition used in this project.

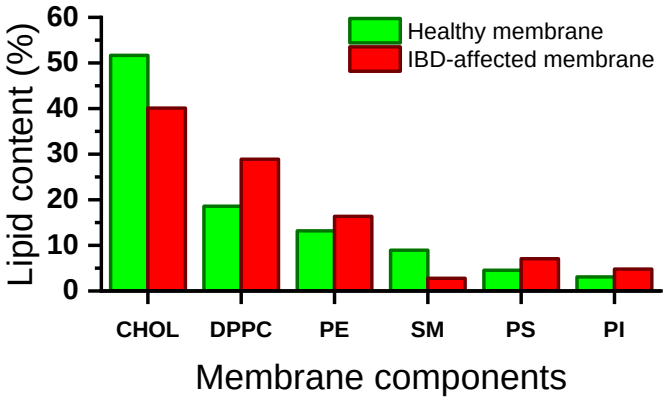

Figure 8. Composition of the outer leaflet of the healthy and IBD-affected membrane models used in this project.

4.3.2 Monolayers of model membranes

First, the Langmuir monolayers for both HM and DM models were prepared, and their π-A isotherms were recorded (Figure 9). From these isotherms, the Ks-π plots were obtained to confirm that the fluidity of the DM aligns well with the literature.

As seen in both Ks-π plots, the DM presents a more fluid nature than the HM model at high surface pressure values, which is in good accordance with the literature regarding the permeability of the plasma membrane of cells in IBD patients. [19,20,21] Table 2 gathers the most relevant features from the π-A isotherms and Ks-π plots for both HM and DM models.

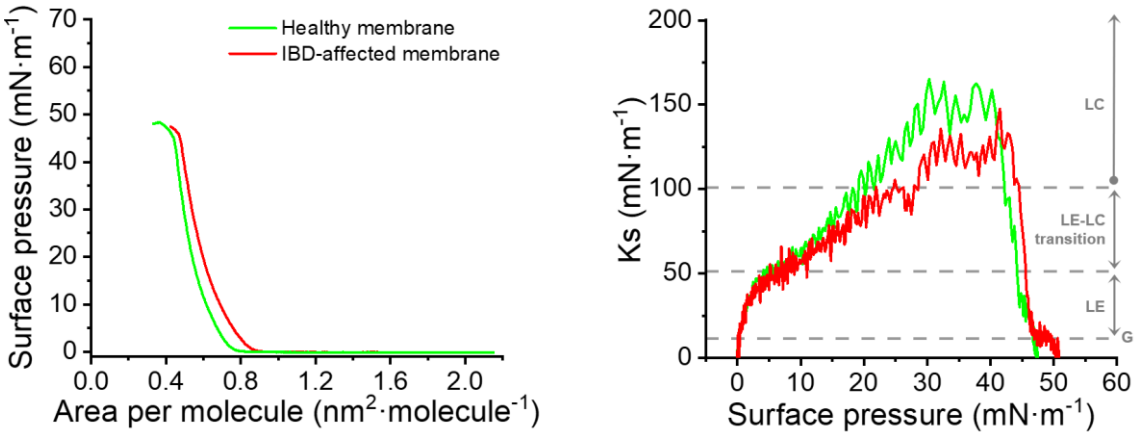

Figure 9. **Left panel:** π-A isotherms for the healthy membrane and IBD-affected membrane monolayers registered at 20±1 ºC. **Right panel:** Ks-π plots the healthy membrane and IBD-affected membrane monolayers.

Table 2. Compilation of the data extracted from the π-A isotherms and respective Ks-π plots of the model membranes.

Model membrane	$A_{LIFT-OFF}$ ($nm^2 \cdot molecule^{-1}$)	$\pi_{G \rightarrow LE}$ ($mN \cdot m^{-1}$)	$\pi_{LE \rightarrow LC}$ ($mN \cdot m^{-1}$)	$\pi_{LC \rightarrow S}$ ($mN \cdot m^{-1}$)	$\pi_{COLLAPSE}$ ($mN \cdot m^{-1}$)	Max Ks ($mN \cdot m^{-1}$)	π max Ks ($mN \cdot m^{-1}$)
HM	0.77	0.22	4.1	18.2	0.38	48.1	165.0
DM	0.89	0.4	5.3	22.0	0.43	47.5	147.5

To obtain further information about the nature of both membrane models, stability experiments were conducted at the air-water interface (Appendix D). During these experiments, the surface pressure was kept constant (with the assistance of automated barrier adjustments), while variations in the area per molecule were recorded over time. In this Master's thesis, a target surface pressure of 30 $mN \cdot m^{-1}$ was chosen, as it is representative of biological membranes. As shown in Appendix D, the HM undergoes less than a 10% decrease in its area per molecule in the first 2 hours of the experiment. After that, the monolayer stabilizes, with minimal changes in the area per molecule over the remaining 13 hours of the experiment. In contrast, the DM exhibits a lower stability, with a ~20% loss in the area per molecule during the first 1.6 hours of the experiment, after which it stabilizes for the rest of the experiment. These results indicate that the HM model is more stable at the biologically relevant surface pressure.

4.3.3 [6]-Gingerol-Model membrane systems

After analysing the monolayers of both membrane models, their interaction with GIN was studied. GIN was mixed with each model membrane at varying molar fractions (χ_{GIN}= 0.05, 0.1, 0.2, 0.3, 0.4, 0.5, 0.6, 0.7, 0.8, and 0.9), with their respective π-A isotherms and Ks-π plots, as shown in Figure 10. For both models, increasing GIN molar fraction enhanced monolayer fluidity. The healthy membrane reached maximum fluidity at χ_{GIN}=0.9. matching that of a single GIN monolayer, whilst the disturbed membrane achieved a similar fluidity at χ_{GIN}=0.8.

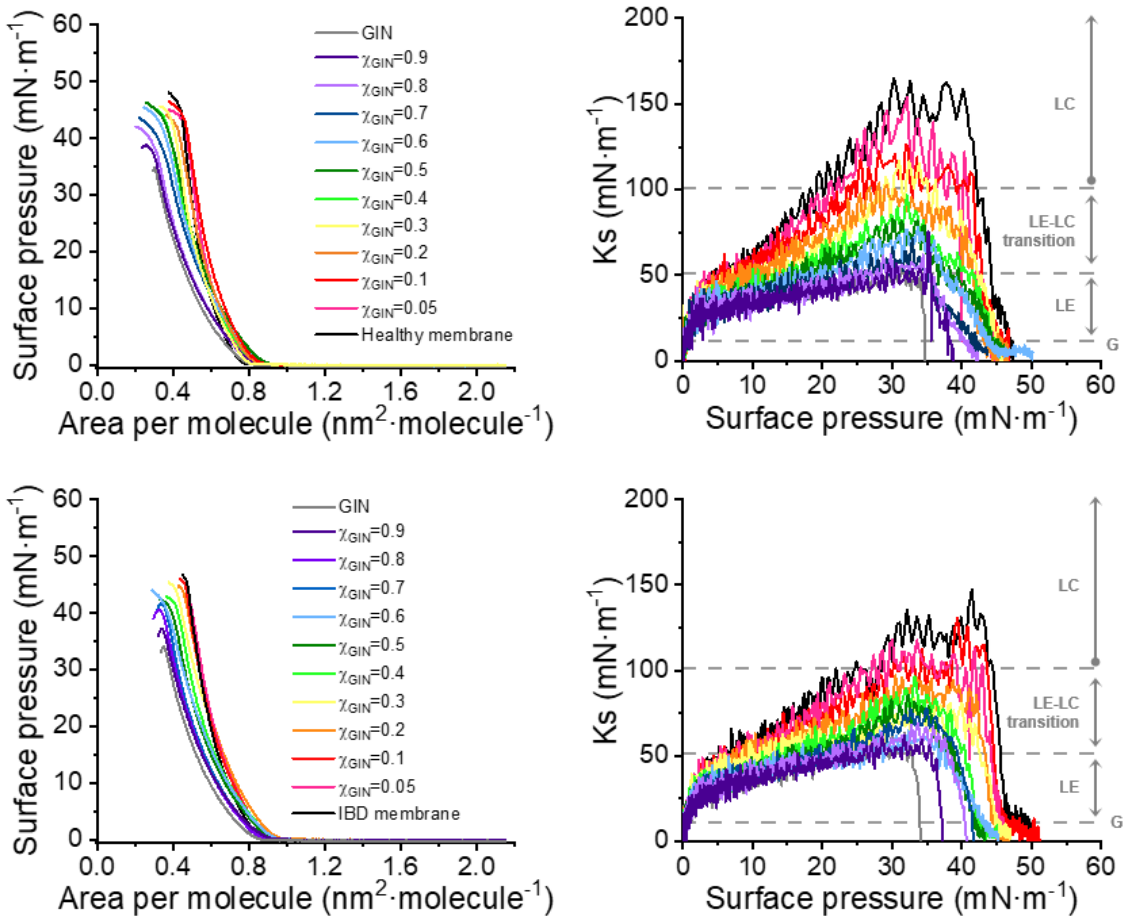

Figure 10. Left panel: π-A isotherms for GIN-HM, and GIN-DM systems recorded at 21 ºC. **Right panel:** Ks-π plots for GIN-HM, and GIN-DM systems.

A thermodynamic study of the both GIN-HM, and GIN-DM systems at the air-water interface was performed. Figure 11 shows the excess area of mixing values for both systems. A^E values are generally positive for all mixtures at each target surface pressure, indicating repulsive interactions between GIN and the membrane components. However, GIN interacts more repulsively with the HM than the DM. In both systems, A^E values decrease with increasing surface pressure, suggesting reduced repulsive interactions at higher surface pressures. The highest A^E values, indicating partially miscible mixtures, are observed for GIN-HM (χ_{GIN}=0.5 at 5 mN·m^{-1}, A^E = 0.090 nm^2·molecule^{-1}), and GIN-DM (χ_{GIN}=0.3 at 5 mN·m^{-1}, A^E = 0.07 nm^2·molecule^{-1}). The lowest A^E values are obtained for GIN-HM (χ_{GIN}=0.8 at 33 mN·m^{-1} , A^E = -0.007 nm^2·molecule^{-1}), and GIN-DM (χ_{GIN}=0.5 at 30 mN·m^{-1}, A^E = -0.009 nm^2·molecule^{-1}).

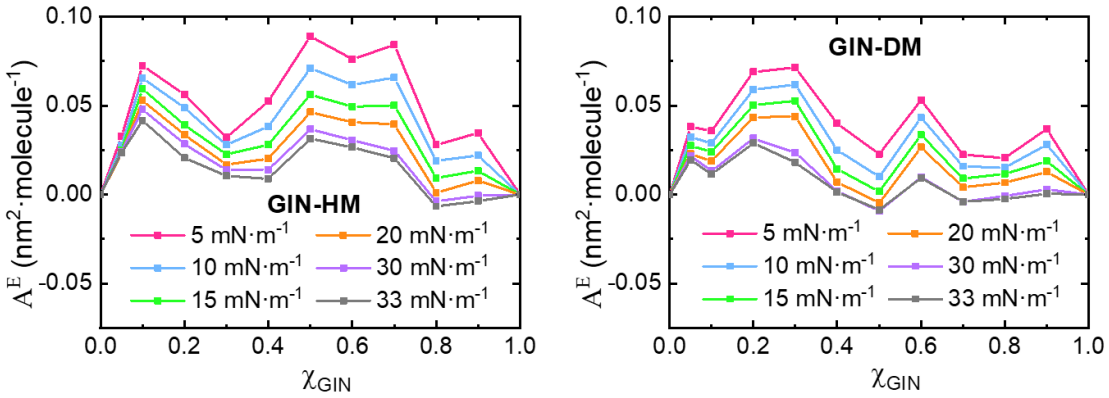

Figure 11. Excess area of mixing vs. GIN molar fraction for GIN-HM (left), and GIN-DM (right) systems.

Figure 12 shows excess Gibbs energy of mixing. ΔG_m^E values are generally positive for all mixtures in both membrane models, indicating repulsive interactions between GIN and the membrane components, these interactions being stronger in the GIN-HM system than in GIN-DM. These results are consistent with the A^E values discussed previously. A remarkable observation in the ΔG_m^E values is trend of increasing ΔG_m^E with surface pressure suggesting that mixtures at higher surface pressures are less thermodynamically favourable. This trend contrasts with the decreasing A^E values observed at higher surface pressures, which indicates less repulsive interactions. This apparent contradiction can be explained by steric accommodation effects of GIN within the membrane components as surface pressure increases, which reduce the value of the excess area, while the energy effects, which are the only ones reflected in ΔG_m^E , continue to show increased repulsion between the components with rising surface pressure. The highest ΔG_m^E values observed correspond to GIN-HM (χ_{GIN}= 0.1 at 33 mN·m^{-1}, ΔG_m^E= 1498 J·mol^{-1}), GIN-HM (χ_{GIN}=0.5 at 33 mN·m^{-1}, ΔG_m^E= 1374 J·mol^{-1}), and GIN-DM (χ_{GIN}=0.3 at 33, ΔG_m^E= 1063 J·mol^{-1}), corresponding to the mixtures with the strongest repulsive interactions between each component. The most favourable mixtures correspond to GIN-HM (χ_{GIN}=0.3 at 5 mN·m^{-1} , ΔG_m^E= 60 J·mol^{-1}), and GIN-DM (χ_{GIN}=0.5 at 30 mN·m^{-1}, ΔG_m^E= 30 J·mol^{-1}), mixture that breaks the trend mentioned formerly.

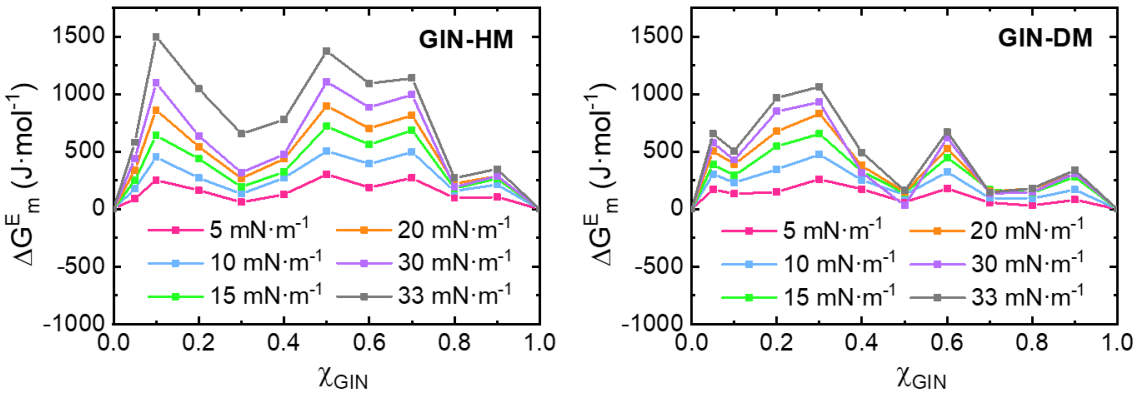

Figure 12. Excess Gibbs energy of mixing vs. GIN molar fraction for GIN-HM (left), and GIN-DM (right) systems.

ΔG_m values are shown in Figure 13. For both systems, ΔG_m values are generally negative, indicating relatively stable monolayers, and ΔG_m values increase with the surface pressure. GIN-DM mixtures seem to be generally more stable than GIN-HM mixtures, since more negative ΔG_m values are observed in the former system. There are some mixtures that present positive ΔG_m values, indicating unstable monolayers: GIN-HM (χ_{GIN}=0.1 at 33 mN·m^{-1}, ΔG_m= 701 J·mol^{-1}), and GIN-DM (χ_{GIN}=0.05 at 33 mN·m^{-1}, ΔG_m= 167 J·mol^{-1}). The most stable mixtures, i.e., the ones with the lowest ΔG_m values are GIN-HM (χ_{GIN}=0.4 at 5 mN·m^{-1}, ΔG_m= -1526 J·mol^{-1}), and GIN-DM (χ_{GIN}=0.5 at 30 mN·m^{-1}, ΔG_m= -1670 J·mol^{-1}).

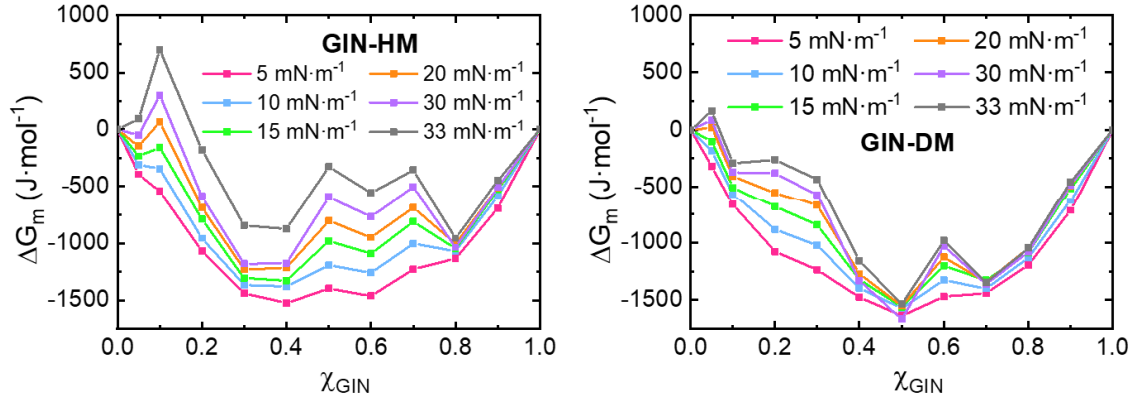

Figure 13. Gibbs energy of mixing vs. GIN molar fraction for GIN-HM (left), and GIN-DM (right) systems.

For comparison purposes, the thermodynamic results at the biological surface pressures for the mixtures of GIN with both model membranes are gathered in Figure 14. As shown in Figure 14a, the GIN-HM system presents generally higher A^E values than the GIN-DM system, meaning that GIN interacts more repulsively with the components in the HM than with those in the DM. Two maxima are observed at χ_{GIN}=0.1 and 0.5.

Moreover, two minima are observed at χ_{GIN}=0.3 and 0.8, corresponding to less repulsion between GIN and HM. As indicated before the presence of several maxima (or minima) in the excess properties figures is a strong indication of phase segregation and poor miscibility. As for the GIN-DM system, the highest repulsion effects occur at χ_{GIN}=0.2 and 0.6. Three minima are observed at χ_{GIN}= 0.1, where there are some repulsive interactions; χ_{GIN}=0.5, where A^E is slightly negative, indicative of the presence of attractive interactions between GIN and DM; and χ_{GIN}=0.7, in which A^E is close to zero, meaning there exists an ideal miscibility. As for ΔG_m^E values (Figure 14b), the positive values obtained further confirm repulsive interactions. The GIN-HM system shows three maxima, indicating mixtures with the highest degree of repulsion, at χ_{GIN}=0.1, 0.5 and 0.7, which are in good agreement with the A^E results. The two minima at χ_{GIN}=0.3 and 0.8 highlight the mixtures with weaker repulsive interactions. Regarding the GIN-DM system, the largest repulsion occurs at χ_{GIN}=0.3 and 0.6, whereas mixtures at χ_{GIN}=0.5 and 0.7 show a close-to-ideal miscibility or immiscibility. Finally, Figure 14c gives insight into the stability of the monolayers at a surface pressure of 30 mN·m^{-1}. Negative ΔG_m values are observed for most of the mixtures, except for GIN-HM at χ_{GIN}=0.1. At low GIN content (χ_{GIN}<0.4), GIN-HM monolayers are more stable than GIN-DM ones. For mixtures at χ_{GIN}=0.4-0.7, GIN-HM mixtures are relatively less stable than GIN-HM ones. At high GIN content (χ_{GIN}>0.7), both systems show an almost identical stability. The most stable composition in the GIN-HM system is located at χ_{GIN}=0.3, whereas the least stable corresponds to χ_{GIN}=0.1. As for the GIN-DM system, the most stable mixture is observed at χ_{GIN}=0.5, and the least stable mixture at χ_{GIN}=0.05, with a slightly positive ΔG_m value.

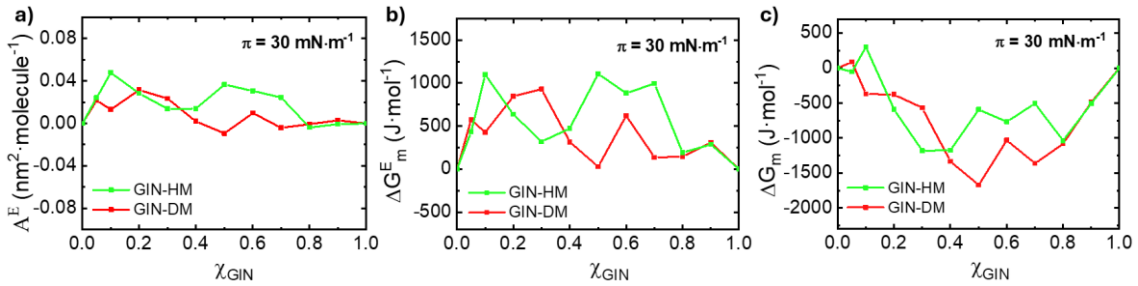

Figure 14. Compilation of thermodynamic parameters for GIN-HM and GIN-DM systems at a surface pressure of 30 mN·m^{-1}: a) Excess area of mixing vs. GIN molar fraction, b) excess Gibbs energy of mixing vs GIN molar fraction, c) Gibbs energy of mixing vs GIN molar fraction.

In order to identify the most thermodynamically favourable mixtures at the biologically relevant surface pressure of 30 $mN \cdot m^{-1}$, the most significant minima for each thermodynamic parameter were compiled in Table 3 for both systems.

Table 3. Compilation of the most miscible and stable mixtures for the GIN-model membranes at 30 $mN \cdot m^{-1}$.

System	χ_{GIN}	A^E ($nm^2 \cdot molecule^{-1}$)	ΔG_m^E ($J \cdot mol^{-1}$)	ΔG_m ($J \cdot mol^{-1}$)
GIN-HM	0.3	0.014	317.8	-1180.4
	0.8	-0.004	190.8	-1036.5
GIN-DM	0.5	-0.009	29.8	-1670.3
	0.7	-0.004	135.2	-1363.0

4.3.4 [6]-Gingerol adsorption experiments

Experiments injecting 20 µL of a GIN solution in ethanol in a concentration of 10^{-4} M and the corresponding blank (20 µL of ethanol) into the subphase were conducted in both of the setups mentioned in the experimental section (**3.2.3**). The GIN solution underwent ultrasonication for 2 minutes to avoid the presence of aggregates before injection. Each experiment was replicated multiple times to verify the reproducibility of the results and had an average duration of 20 hours. The obtained results are shown in Figure 15.

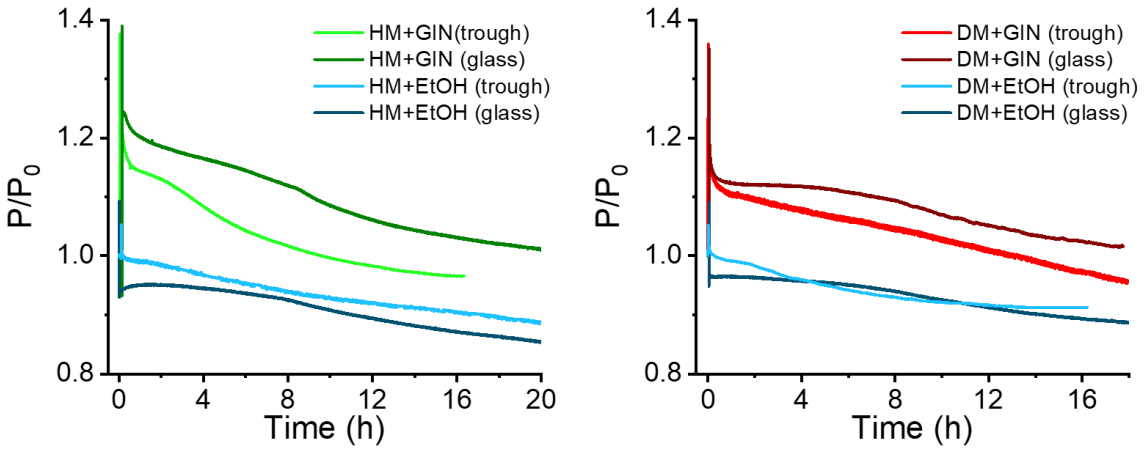

Figure 15. Surface pressure variation expressed as the surface pressure recorded after GIN or EtOH injection, P, divided by the surface pressure before injection, P_0, for the HM system (left) and the DM system (right) for the indicated setups.

As seen in Figure 15, the first noticeable feature in all the registered plots is that at the time of injection, t = 0 h, the surface pressure increases in a different extent

depending on the solution injected and the model membrane used. This increase in surface pressure is much less significant in the blanks (ethanol injection) than in the experiments where a GIN solution in ethanol is injected. This suggests that GIN molecules are capable of resurfacing and penetrating into both model membranes.

In all cases, a decrease in the surface pressure value after injection occurs, which is more significant in GIN experiments rather than for the blanks. This can be explained due to the nature of GIN: as mentioned previously, GIN tends to fluidize monolayers, leading to a decrease in the stability of the model membranes.

Another observation is that when comparing experiments done in the different setups, there is a significative difference in the stabilized surface pressure after injection for both GIN and EtOH experiments. This suggests that there is a certain degree of diffusion of the molecules injected in the subphase in the experiments done in the trough.

When comparing experiments done in the same setup, one relevant observation is that the increase in surface pressure is slightly greater when injecting GIN in the HM compared to the DM. This might seem contradictory when considering the fluidity of both systems, as the HM is more condensed and, therefore, could be considered as more resistant to the penetration of additional molecules. However, this effect can be attributed to the different levels of repulsive interactions between GIN and each monolayer. As shown previously, at χ_{GIN}=0.3, the repulsive interactions between GIN and DM are stronger than those between in GIN and HM.

Additionally, a difference in the drop in the surface pressure immediately after the injection of GIN is observed between the two model membranes. The magnitude of this drop is smaller for the HM membrane than for the DM membrane. This can be explained by the fluidity of each model membrane. As discussed previously, at a surface pressure of 30 $mN \cdot m^{-1}$, the HM is more compact than the DM (with Ks values of 165.0 $mN \cdot m^{-1}$ vs 105.5 $mN \cdot m^{-1}$), meaning that when GIN is introduced into the monolayer, the fluidity of the HM remains lower than that of the DM. Another possible contributing factor is the repulsive interactions between GIN and the model membranes. As shown in the previous thermodynamic analysis of GIN-model membrane systems, at χ_{GIN}=0.3 and a surface pressure of 30 $mN \cdot m^{-1}$, the excess area and excess Gibbs energy of mixing indicate a stronger repulsion between GIN and the DM than in the GIN-HM system. This suggests a lower penetration of the GIN molecules in the case of the DM, which could contribute

to the observed drop in the surface pressure following the injection of GIN, in addition to the fluidization effect.

In order to verify the penetration of GIN in the membranes, an additional experiment injecting a lower content of GIN (χ_{GIN}=0.1) into the DM was conducted and compared to previous experiments. As shown in Figure 16, a smaller increase in the surface pressure when injecting a lower content in GIN is observed. Additionally, the stabilized surface pressure is similar for injections of GIN at χ_{GIN}=0.1 and 0.3, which might appear contradictory at first glance, but aligns well with the hypothesis suggesting the repulsion of GIN molecules from the DM. This is because, at χ_{GIN}=0.1, as indicated in the thermodynamic analysis, the repulsive interactions between GIN and DM are weaker than at χ_{GIN}=0.3. The Gibbs energy of mixing further supports this observation, showing that the monolayer formed after injection at χ_{GIN}=0.1 is less stable than at χ_{GIN}=0.3.

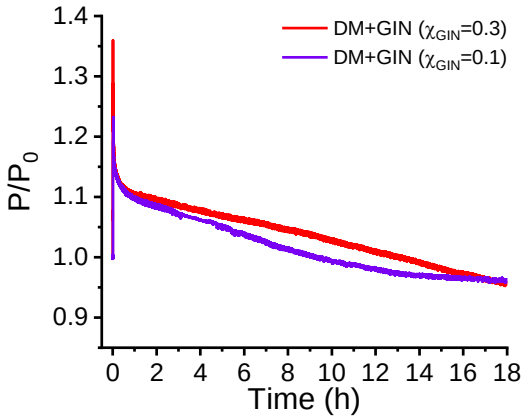

Figure 16. GIN adsorption experiments with the DM, performed in the mini trough, at the indicated molar fractions of GIN.

In conclusion, these experiments provide strong evidence that GIN successfully penetrates both the DM and HM model membranes. In addition, these findings highlight the presence of a diffusion effect inherent to the trough experimental setup.

4.3.5 Brewster angle microscopy (BAM)

To further confirm the penetration of GIN in the model cell membranes, Brewster Angle Microscope (BAM) experiments were performed to visualize the monolayer formation of the HM and the DM *in situ*. As depicted in Figure 17, images A1 and B1 show the initial state of the monolayer, in which the membrane is in a G phase. With increasing surface pressure, the monolayer becomes more compact, resulting in progressively brighter images. In image B4, corresponding to the DM monolayer, some domains (brightest areas) and holes (darkest areas) are visible, indicating a less ordered

state compared to the HM at the same surface pressure, which appears homogeneous. This observation is in good agreement with the Ks values obtained for both monolayers at the indicated surface pressure: at 25 $mN \cdot m^{-1}$, the HM is in a LC state whereas the DM is still in a LE-LC transition state.

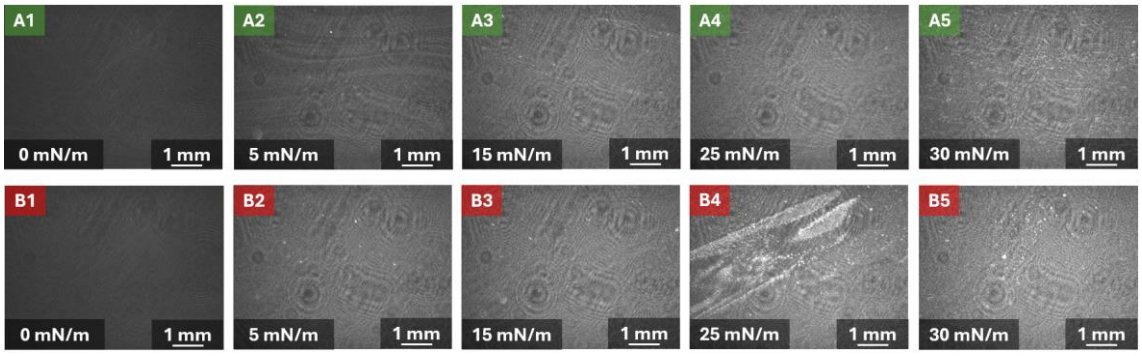

Figure 17. BAM images for HM (A1-A5), and DM (B1-B5) monolayers at the indicated surface pressure values.

Additionally, BAM was used to prove the introduction of GIN molecules from the subphase into the monolayers. Blank experiments using ethanol were carried out for comparison. Figure 18 shows BAM images of the adsorption experiments for the HM with the injection of GIN (χ_{GIN}=0.3; B series), and the corresponding blank experiment (A series). In the first row of images, a slight increase in the brightness of the image occurs immediately after the injection of EtOH. Then, the brightness decreases slightly after one hour, consistent with the results in Figure 15, which demonstrated that EtOH injection destabilises the monolayer, resulting in a more fluid monolayer. In contrast, the second row of images, corresponding to the injection of GIN beneath the HM monolayer, exhibits noticeable increase in the brightness of the images over time. Starting from image B3, the appearance of distinct bright domains, absent in the blank experiment, indicates the successful penetration of GIN into the monolayer.

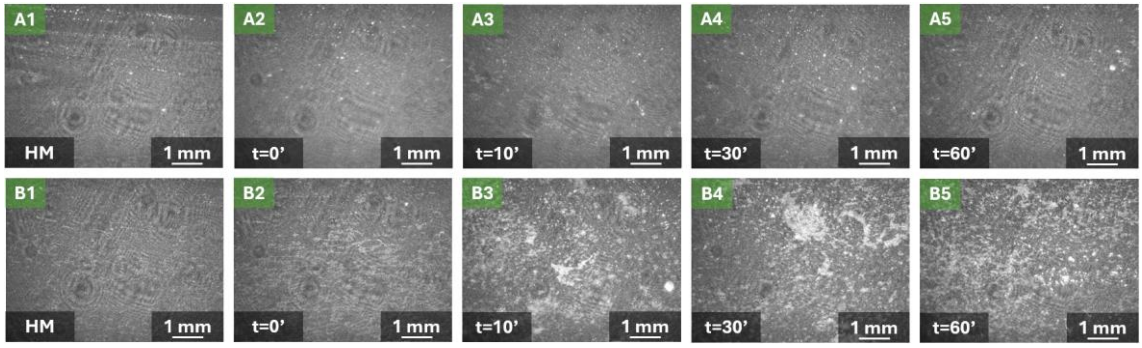

Figure 18. BAM images for the HM monolayer with EtOH injection (A1-A5), and the HM monolayer with GIN injection (B1-B5) at the indicated time after injection.

Figure 19 presents the BAM experiment results for the DM membrane. In the first row of images, corresponding to the blank experiment with EtOH injection, a similar result as the blank experiment for the HM is obtained. However, the second row of images, corresponding to the injection of GIN (χ_{GIN}=0.3) beneath the DM membrane, an increase in the brightness of the images is observed after injection. In B2, at t=0', there is a clear presence of domains attributed to the incorporation of GIN into the HM membrane. Additionally, darker areas in the monolayer suggest disruptions, which are tentatively attributed here to the physical disturbance caused by introducing the syringe into the water subphase or even to phase segregation induced by GIN. In B3, more domains are observed suggesting phase segregation between the GIN domains and the DM monolayer. This segregation is more evident than in the HM experiments and can be attributed to stronger repulsive interactions between GIN and the DM membrane compared to HM. In the latter case, the weaker repulsive forces allow for better miscibility of GIN with the monolayer molecules, previously demonstrated in Figure 11. 60 minutes after the injection, the monolayer exhibits a more heterogeneous appearance, with the presence of some domains and uncovered areas. This observation is consistent with the Ks values obtained in the above analysis for DM membranes in the presence of GIN, supporting the notion of a less compact and less stable DM monolayer in the presence of GIN.

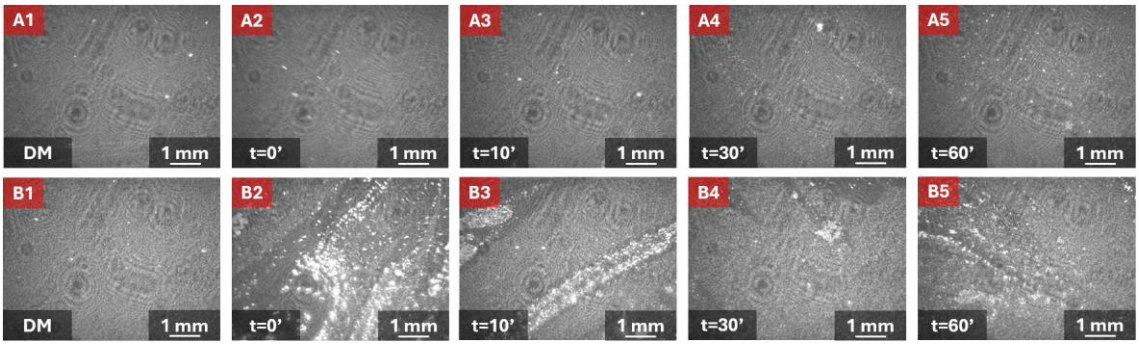

Figure 19. BAM images for the DM monolayer with EtOH injection (A1-A5), and the DM monolayer with GIN injection (B1-B5) at the indicated time after injection.

An additional control experiment to fully confirm GIN penetration in the HM and DM membranes and rule out EtOH effects was performed. Specifically, BAM images were captured following the injection of both substances in the subphase, in the absence of a model membrane monolayer at the air-water interface. Results are shown in Figure 20. As shown in A1-A5 images, corresponding to the injection of EtOH, there was no significant change in the brightness of the images, nor were any structures visible. At the

time of injection, the surface pressure increased to 0.8 $mN \cdot m^{-1}$. In contrast, the injection of an equivalent volume of a GIN solution, resulted in the appearance of visible structures in the recorded images, as seen in B1-B5 images. Additionally, immediately after injection, the recorded surface pressure was of 1.5 $mN \cdot m^{-1}$, higher than the recorded value for EtOH. These results show unequivocable proof of the behaviour of GIN behaviour, demonstrating its tendency to migrate and concentrate at the air-water interface.

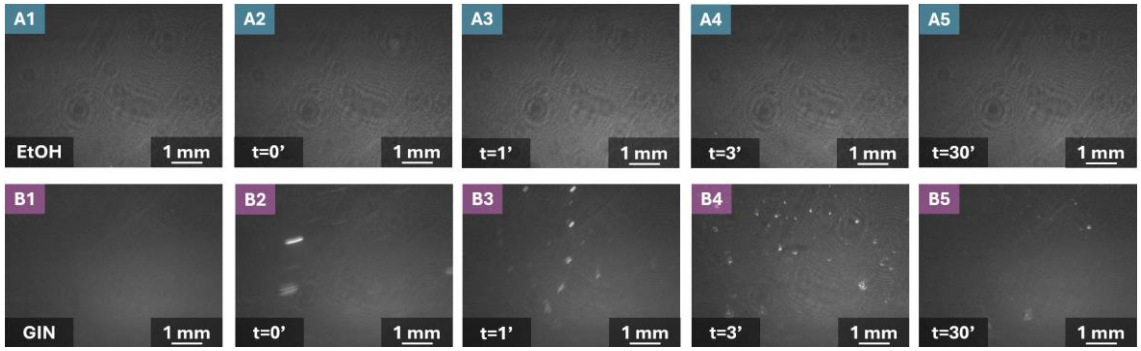

Figure 20. BAM images of a clean water surface (A1, B1), and when injecting the same volume of EtOH (A1-A5) and GIN (B1-B5) in the subphase as a function of time.

In conclusion, these experiments demonstrate the ability of GIN to incorporate into the model membranes.

5. Summary and conclusions

This Master's Thesis investigates the interactions of [6]-Gingerol (GIN), with model cell membranes prepared using the Langmuir technique. Model membranes mimicking both healthy colonocyte plasma membranes and those affected by inflammatory bowel disease (IBD) were prepared. As a preliminary study, single monolayers of each model membrane component, as well as GIN, were obtained, analysing the information extracted from the π-A isotherms and respective Ks-plots. Then, binary mixtures based on GIN mixed with each of the model membrane components were prepared at the air-water interface at different molar fractions of GIN, which were rigorously studied by means of thermodynamic analysis. This approach provided insights into the miscibility and stability of the mixtures, revealing that GIN induces fluidization in all single-component monolayers. This effect was most pronounced in CHOL, DPPC, and SM monolayers. Additionally, GIN exhibited a specific affinity for CHOL and SM, as evidenced by favourable thermodynamic properties.

Building on this understanding, complex model membranes representing the plasma membranes of both healthy and IBD-affected colonocytes. The incorporation of GIN at various molar fractions was evaluated. The results demonstrated that GIN fluidizes the membrane monolayers in a concentration-dependent manner. Thermodynamic analysis at a biologically relevant surface pressure of 30 $mN \cdot m^{-1}$ highlighted key differences in membrane behaviour. Mixtures with higher GIN content were more miscible and stable in the DM, whereas lower GIN content presented generally more thermodynamically favoured mixtures in the HM (except at χ_{GIN}=0.1).

For a better understanding of the biological relevance of GIN penetration through cell membranes, the capability of GIN to adsorb into the model membranes, simulating the biological adsorption from the bloodstream into the intestinal epithelium, was studied and visualized *in situ* by means of BAM. It has been concluded that GIN does in fact penetrate both the HM and DM, and that at χ_{GIN}=0.3, the incorporation of GIN into the membrane seems more favourable in the HM, which is in good agreement with the conclusions extracted from the thermodynamic analysis, as less repulsive interactions were observed between the HM than in the DM at that χ_{GIN} value. However, by consideration of only BAM images, it remains challenging to quantify the extent of GIN incorporation in each membrane or determine whether this incorporation results in phase segregation and/or integration of GIN within the components of the membrane. Thus, for future perspectives, additional characterization is needed for this purpose. This thesis is hoped to serve as a preliminary study of GIN-containing-liposome formulation for the development of more biocompatible drugs for IBD, as well as other diseases.

References

(1) Nelson, D. L.; Cox, M. M. *Lehninger Principles of Biochemistry, 4th Edition*.

(2) Overington, J. P.; Al-Lazikani, B.; Hopkins, A. L. How Many Drug Targets Are There? *Nat Rev Drug Discov* **2006**, *5* (12), 993–996. https://doi.org/10.1038/nrd2199.

(3) Alves, A. C.; Ribeiro, D.; Nunes, C.; Reis, S. Biophysics in Cancer: The Relevance of Drug-Membrane Interaction Studies. *Biochimica et Biophysica Acta (BBA) - Biomembranes* **2016**, *1858* (9), 2231–2244. https://doi.org/10.1016/j.bbamem.2016.06.025.

(4) Coronado, S.; Herrera, J.; Pino, M. G.; Martín, S.; Ballesteros-Rueda, L.; Cea, P. Advancements in Engineering Planar Model Cell Membranes: Current Techniques, Applications, and Future Perspectives. *Nanomaterials* **2024**, *14* (18), 1489. https://doi.org/10.3390/nano14181489.

(5) Oliveira, O. N.; Caseli, L.; Ariga, K. The Past and the Future of Langmuir and Langmuir–Blodgett Films. *Chemical Reviews* **2022**, *122* (6), 6459–6513. https://doi.org/10.1021/acs.chemrev.1c00754.

(6) Luchini, A.; Vitiello, G. Mimicking the Mammalian Plasma Membrane: An Overview of Lipid Membrane Models for Biophysical Studies. *Biomimetics* **2020**, *6* (1), 3. https://doi.org/10.3390/biomimetics6010003.

(7) Ruiz-Rincón, S.; González-Orive, A.; De La Fuente, J. M.; Cea, P. Reversible Monolayer-Bilayer Transition in Supported Phospholipid LB Films under the Presence of Water: Morphological and Nanomechanical Behavior. *Langmuir* **2017**, *33* (30), 7538–7547. https://doi.org/10.1021/acs.langmuir.7b01268.

(8) Dotor, L.; García-Pinilla, J. M.; Martín, S.; Cea, P. Langmuir and Langmuir-Blodgett Technologies as Nanoarchitectonic Tools for the Incorporation of Curcumin in Membrane Systems. *Nanoscale* **2023**, *15* (6), 2891–2903. https://doi.org/10.1039/d2nr06631a.

(9) Hecht, G. A. *Microbial Pathogenesis and the Intestinal Epithelial Cell*; 2003.

(10) Laukoetter, M. G.; Nava, P.; Nusrat, A. Role of the Intestinal Barrier in Inflammatory Bowel Disease. *World J Gastroenterol* **2008**, *14* (3), 401–407. https://doi.org/10.3748/wjg.14.401.

(11) Litvak, Y.; Byndloss, M. X.; Bäumler, A. J. Colonocyte Metabolism Shapes the Gut Microbiota. *Science (1979)* **2018**, *362* (6418). https://doi.org/10.1126/science.aat9076.

(12) Baumgart, D. C.; Sandborn, W. J. Crohn's Disease. *The Lancet* **2012**, *380* (9853), 1590–1605. https://doi.org/10.1016/s0140-6736(12)60026-9.

(13) Rajapakse, R. *Inflammatory Bowel Disease : Pathogenesis, Diagnosis and Management*; Springer: Cham, Switzerland, 2021.

(14) Peyrin-Biroulet, L.; Loftus, E. V.; Colombel, J.-F.; Sandborn, W. J. The Natural History of Adult Crohn's Disease in Population-Based Cohorts. *American Journal of Gastroenterology* **2010**, *105* (2), 289–297. https://doi.org/10.1038/ajg.2009.579.

(15) Mishra, R.; Dhawan, P.; Srivastava, A. S.; Singh, A. B. Inflammatory Bowel Disease: Therapeutic Limitations and Prospective of the Stem Cell Therapy. *World J Stem Cells* **2020**, *12* (10), 1050–1066. https://doi.org/10.4252/wjsc.v12.i10.1050.

(16) Michielan, A.; D'Incà, R. Intestinal Permeability in Inflammatory Bowel Disease: Pathogenesis, Clinical Evaluation, and Therapy of Leaky Gut. *Mediators of Inflammation* **2015**, *2015*, 1–10. https://doi.org/10.1155/2015/628157

(17) Scoville, E. A.; Allaman, M. M.; Brown, C. T.; Motley, A. K.; Horst, S. N.; Williams, C. S.; Koyama, T.; Zhao, Z.; Adams, D. W.; Beaulieu, D. B.; Schwartz, D. A.; Wilson, K. T.; Coburn, L. A. Alterations in Lipid, Amino Acid, and Energy Metabolism Distinguish Crohn's Disease from Ulcerative Colitis and Control Subjects by Serum Metabolomic Profiling. *Metabolomics* **2018**, *14* (1). https://doi.org/10.1007/s11306-017-1311-y.

(18) Diab, J.; Hansen, T.; Goll, R.; Stenlund, H.; Ahnlund, M.; Jensen, E.; Moritz, T.; Florholmen, J.; Forsdahl, G. Lipidomics in Ulcerative Colitis Reveal Alteration in Mucosal Lipid Composition Associated with the Disease State. *Inflamm Bowel Dis* **2019**, *25* (11), 1780–1787. https://doi.org/10.1093/ibd/izz098.

(19) Ehehalt, R.; Wagenblast, J.; Erben, G.; Lehmann, W. D.; Hinz, U.; Merle, U.; Stremmel, W. Phosphatidylcholine and Lysophosphatidylcholine in Intestinal Mucus of Ulcerative Colitis Patients. A Quantitative Approach by Nanoelectrospray-Tandem Mass Spectrometry. *Scand J Gastroenterol* **2004**, *39* (8), 737–742. https://doi.org/10.1080/00365520410006233.

(20) Aozaki, S. Decreased Membrane Fluidity in Erythrocytes from Patients with Crohn's Disease. *Gastroenterologia Japonica* **1989**, *24* (3), 246–254. https://doi.org/10.1007/bf02774321.

(21) Bauer, J.; Liebisch, G.; Hofmann, C.; Huy, C.; Schmitz, G.; Obermeier, F.; Bock, J. Lipid Alterations in Experimental Murine Colitis: Role of Ceramide and Imipramine for Matrix Metalloproteinase-1 Expression. *PLoS One* **2009**, *4* (9). https://doi.org/10.1371/journal.pone.0007197.

(22) Bode Ann M.; Dong Zigang. The Amazing and Mighty Ginger. In *Herbal Medicine: Biomolecular and Clinical Aspects. 2nd edition.*; 2011.

(23) Chang, K. W.; Kuo, C. Y. 6-Gingerol Modulates Proinflammatory Responses in Dextran Sodium Sulfate (DSS)-Treated Caco-2 Cells and Experimental Colitis in Mice through Adenosine Monophosphate-Activated Protein Kinase (AMPK) Activation. *Food Funct* **2015**, *6* (10), 3334–3341. https://doi.org/10.1039/c5fo00513b.

(24) Brown, A. C.; Shah, C.; Liu, J.; H Pham, J. T.; Gang Zhang, J.; Jadus, M. R. Ginger's (Zingiber Officinale Roscoe) Inhibition of Rat Colonic Adenocarcinoma Cells Proliferation and Angiogenesis In Vitro. *Phytother. Res* **2009**, *23*, 640–645. https://doi.org/10.1002/ptr.

(25) Prasad, S.; Tyagi, A. K. Ginger and Its Constituents: Role in Prevention and Treatment of Gastrointestinal Cancer. *Gastroenterology Research and Practice* **2015**, *2015*, 1–11. https://doi.org/10.1155/2015/142979.

(26) Furlan, V.; Bren, U. Protective Effects of [6]-Gingerol against Chemical Carcinogens: Mechanistic Insights. *Int J Mol Sci* **2020**, *21* (3). https://doi.org/10.3390/ijms21030695.

(27) de Lima, R. M. T.; dos Reis, A. C.; de Menezes, A. A. P. M.; Santos, J. V. de O.; Filho, J. W. G. de O.; Ferreira, J. R. de O.; de Alencar, M. V. O. B.; da Mata, A. M. O. F.; Khan, I. N.; Islam, A.; Uddin, S. J.; Ali, E. S.; Islam, M. T.; Tripathi, S.; Mishra, S. K.; Mubarak, M. S.; Melo-Cavalcante, A. A. de C. Protective and Therapeutic Potential of Ginger (Zingiber Officinale) Extract and [6]-Gingerol in Cancer: A Comprehensive Review. *Phytotherapy Research : PTR* **2018**, *32* (10), 1885–1907. https://doi.org/10.1002/ptr.6134.

(28) Alharbi, K. S.; Nadeem, M. S.; Afzal, O.; Alzarea, S. I.; Altamimi, A. S. A.; Almalki, W. H.; Mubeen, B.; Iftikhar, S.; Shah, L.; Kazmi, I. Gingerol, a Natural Antioxidant, Attenuates Hyperglycemia and Downstream Complications. *Metabolites* **2022**, *12* (12), 1274. https://doi.org/10.3390/metabo12121274.

(29) Wang, S.; Zhang, C.; Yang, G.; Yang, Y. Biological Properties of 6-Gingerol: A Brief Review. *Natural Product Communications* **2014**, *9* (7), 1027–1030.

(30) Abdel Gawad, H.; Hammad, L.; El-Abhar, H. Amelioration of Acetic Acid-Induced Colitis in Rats by Oral Administration of Ginger Extract. *Bulletin of Egyptian Society for Physiological Sciences* **2007**, *27* (1), 221–240. https://doi.org/10.21608/besps.2007.37138.

(31) Zhang, M.; Viennois, E.; Prasad, M.; Zhang, Y.; Wang, L.; Zhang, Z.; Han, M. K.; Xiao, B.; Xu, C.; Srinivasan, S.; Merlin, D. Edible Ginger-Derived Nanoparticles: A Novel Therapeutic Approach for the Prevention and Treatment of Inflammatory Bowel Disease and Colitis-Associated Cancer. *Biomaterials* **2016**, *101*, 321–340. https://doi.org/10.1016/j.biomaterials.2016.06.018.

(32) Sang, S.; Snook, H. D.; Tareq, F. S.; Fasina, Y. Precision Research on Ginger: The Type of Ginger Matters. *J Agric Food Chem* **2020**, *68* (32), 8517–8523. https://doi.org/10.1021/acs.jafc.0c03888.

(33) Man, F.; Meng, C.; Liu, Y.; Wang, Y.; Zhou, Y.; Ma, J.; Lu, R. The Study of Ginger-Derived Extracellular Vesicles as a Natural Nanoscale Drug Carrier and Their Intestinal Absorption in Rats. *AAPS PharmSciTech* **2021**, *22* (6). https://doi.org/10.1208/s12249-021-02087-7.

(34) Thangavelu, P.; Sundaram, V.; Gunasekaran, K.; Mujyambere, B.; Raju, S.; Kannan, A.; Arasu, A.; Krishna, K.; Ramamoorthi, J.; Ramasamy, S.; Velusamy, T.; Samiappan, S. Development of Optimized Novel Liposome Loaded with 6-Gingerol and Assessment of Its Therapeutic Activity against NSCLC in Vitro and in Vivo Experimental Models. *Chemistry and Physics of Lipids* **2022**, *245*, 105206. https://doi.org/10.1016/j.chemphyslip.2022.105206.

(35) Ghazwani, M.; Alqarni, M. H.; Hani, U.; Alam, A. QbD-Optimized, Phospholipid-Based Elastic Nanovesicles for the Effective Delivery of 6-Gingerol: A Promising Topical Option for Pain-Related Disorders. *Int J Mol Sci* **2023**, *24* (12), 9983. https://doi.org/10.3390/ijms24129983.

(36) Adwan, L., Fabricación de membranas celulares artificiales y evaluación de sus propiedades para aplicaciones en el campo de la salud, Trabajo de Fin de Grado; 2023.

(37) Adwan, L.; Dotor, L.; Pino, M. G.; Gil, A.; Martin, S.; Cea, P. Interfacial Insights: [6]-Gingerol Monolayers at the Air-Water Interface and Beyond. *Heliyon* **2024**, *10* (20). https://doi.org/10.1016/j.heliyon.2024.e39350.

(38) Adamson, A. W.; Gast, A.P. *Physical Chemistry of Surfaces*, 6th ed.; Wiley: New York, 1997

(39) Pagano, R. E.; Gershfeld, N. L. Physical Chemistry of Lipid Films at the Air-Water Interface. II. Binary Lipid Mixtures. Principles Governing Miscibility of Lipids in Surfaces. **1972**, *76* (9), 1238–1243. https://doi.org/10.1021/j100653a002.

(40) Haro, M.; Cea, P.; Gascón, I.; Royo, F. M.; López, M. C. Mixed Langmuir and Langmuir-Blodgett Films of a Proton Sponge and a Fatty Acid: Influence of the Subphase Nature on the Interactions between the Two Components. *Journal of Physical Chemistry B* **2007**, *111* (11), 2845–2855. https://doi.org/10.1021/jp065954b.

(41) P. Dynarowicz-Łątka; K. Kita. Molecular Interaction in Mixed Monolayers at the Air-Water Interface. *Adv Colloid Interface Sci* **1999**, *79* (1), 1–17. https://doi.org/https://doi.org/10.1016/S0001-8686(98)00064-5.

(42) Davies, J. T.; Rideal, E. K. *Interfacial Phenomena*; Academic Press: New York, 1963.

(43) Marsh, D. *Lateral Pressure in Membranes*; 1996; Vol. 1286.

(44) Kaganer, V. M.; Möhwald, H.; Dutta, P. Structure and Phase Transitions in Langmuir Monolayers. *Reviews of Modern Physics* **1999**, *71* (3), 779–819. https://doi.org/10.1103/revmodphys.71.779.

(45) Hoenig, D.; Moebius, D. Direct Visualization of Monolayers at the Air-Water Interface by Brewster Angle Microscopy. *The Journal of Physical Chemistry* **1991**, *95* (12), 4590–4592. https://doi.org/10.1021/j100165a003.

(46) Blois, A.; Holmsen, H.; Martino, G.; Corti, A.; Metz-Boutigue, M. H.; Helle, K. B. Interactions of Chromogranin A-Derived Vasostatins and Monolayers of Phosphatidylserine, Phosphatidylcholine and Phosphatidylethanolamine. *Regul Pept* **2006**, *134* (1), 30–37. https://doi.org/10.1016/j.regpep.2005.11.003.

(47) Toimil, P.; Prieto, G.; Miñones, J.; Sarmiento, F. A Comparative Study of F-DPPC/DPPC Mixed Monolayers. Influence of Subphase Temperature on F-DPPC and DPPC Monolayers. *Physical Chemistry Chemical Physics* **2010**, *12* (40), 13323–13332. https://doi.org/10.1039/c0cp00506a.

(48) Żak, A.; Korshunova, K.; Rajtar, N.; Kulig, W.; Kepczynski, M. Deciphering Lipid Arrangement in Phosphatidylserine/Phosphatidylcholine Mixed Membranes: Simulations and Experiments. *Langmuir* **2023**, *39* (51), 18995–19007. https://doi.org/10.1021/acs.langmuir.3c03061.

(49) Haro, M.; Giner, B.; Lafuente, C.; López, M. C.; Royo, F. M.; Cea, P. Proton Sponge and Fatty Acid Interactions at the Air-Water Interface. Thermodynamic, Spectroscopic, and Microscopic Study. *Langmuir* **2005**, *21* (7), 2796–2803. https://doi.org/10.1021/la047171s.

(50) Bestard-escalas, J.; Maimó-barceló, A.; Lopez, D. H.; Reigada, R.; Guardiola-serrano, F.; Ramos-vivas, J.; Hornemann, T.; Okazaki, T.; Barceló-coblijn, G. Common and Differential Traits of the Membrane Lipidome of Colon Cancer Cell Lines and Their Secreted Vesicles: Impact on Studies Using Cell Lines. *Cancers (Basel)* **2020**, *12* (5). https://doi.org/10.3390/cancers12051293.

(51) Van Meer, G.; Voelker, D. R.; Feigenson, G. W. Membrane Lipids: Where They Are and How They Behave. *Nature Reviews Molecular Cell Biology* **2008**, *9* (2), 112–124. https://doi.org/10.1038/nrm2330.

(52) Forstner, G. G.; Tanaka, K.; Isselbacher, K. J. Lipid Composition of the Isolated Rat Intestinal Microvillus Membrane. *Biochemical Journal* **1968**, *109* (1), 51–59. https://doi.org/10.1042/bj1090051.

(53) Zachowski, A. Phospholipids in Animal Eukaryotic Membranes: Transverse Asymmetry and Movement. *Biochemical Journal* **1993**, *294* (1), 1–14. https://doi.org/10.1042/bj2940001.

(54) Marquardt, D.; Geier, B.; Pabst, G. Asymmetric Lipid Membranes: Towards More Realistic Model Systems. *Membranes* **2015**, *5* (2), 180–196. https://doi.org/10.3390/membranes5020180.

(55) Yesylevskyy, S. O.; Demchenko, A. P. How Cholesterol Is Distributed between Monolayers in Asymmetric Lipid Membranes. *European Biophysics Journal* **2012**, *41* (12), 1043–1054. https://doi.org/10.1007/s00249-012-0863-z.

(56) Birge, R. B.; Boeltz, S.; Kumar, S.; Carlson, J.; Wanderley, J.; Calianese, D.; Barcinski, M.; Brekken, R. A.; Huang, X.; Hutchins, J. T.; Freimark, B.; Empig, C.; Mercer, J.; Schroit, A. J.; Schett, G.; Herrmann, M. Phosphatidylserine Is a Global Immunosuppressive Signal in Efferocytosis, Infectious Disease, and Cancer. *Cell Death and Differentiation*. Nature Publishing Group June 1, **2016**, pp 962–978. https://doi.org/10.1038/cdd.2016.11.

(57) Nunes, T.; Bernardazzi, C.; de Souza, H. S. Cell Death and Inflammatory Bowel Diseases: Apoptosis, Necrosis, and Autophagy in the Intestinal Epithelium. *BioMed Research International* **2014**, *2014*, 1–12. https://doi.org/10.1155/2014/218493.

Appendix A

Photograph of the Langmuir trough (KSV Nima KN 2003, 580x145 mm^2) used for the preparation of model cell membrane and recording of the π-A isotherms in this project. Parts of the used KSV trough: a) Teflon® trough; b) mobile polyoxymethylene barriers; c) Wilhelmy balance; d) Wilhelmy plate; e) Dipping well; f) Dipping arm.

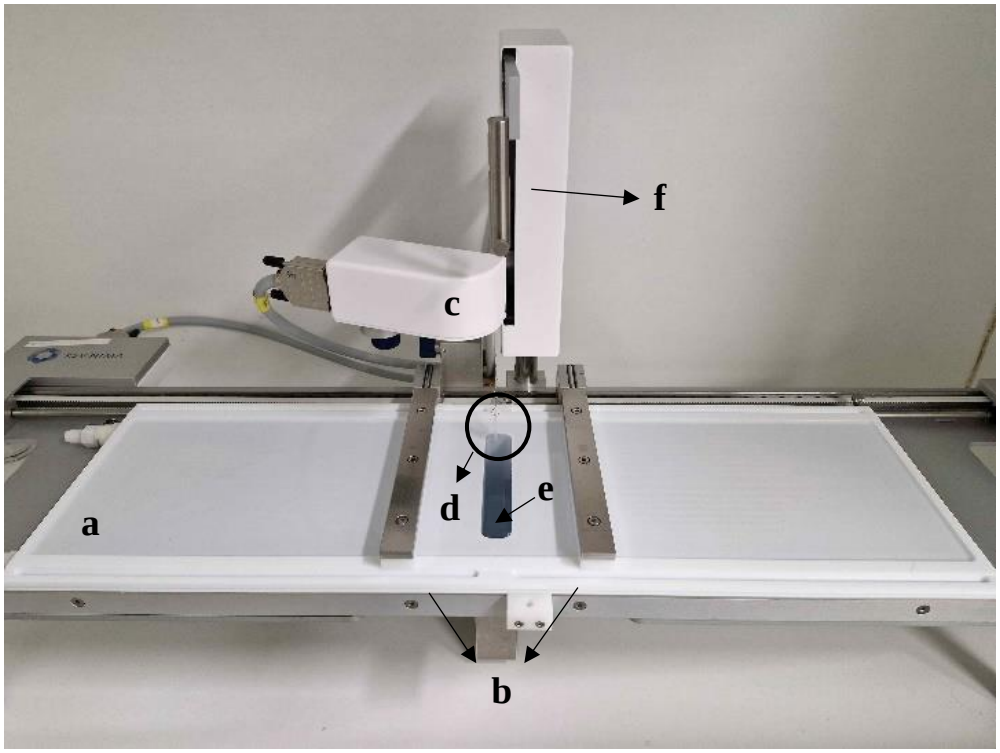

Appendix B

Setup used for the BAM experiments. A mini-Brewster angle microscopy (mini-BAM) from Nanofilm Technologie GmbH was used. The setup includes the following parts: a) Wilhelmy balance; b) mini-Brewster angle microscope; c) Wilhelmy plate: d) light trap; e) glass Petri dish.

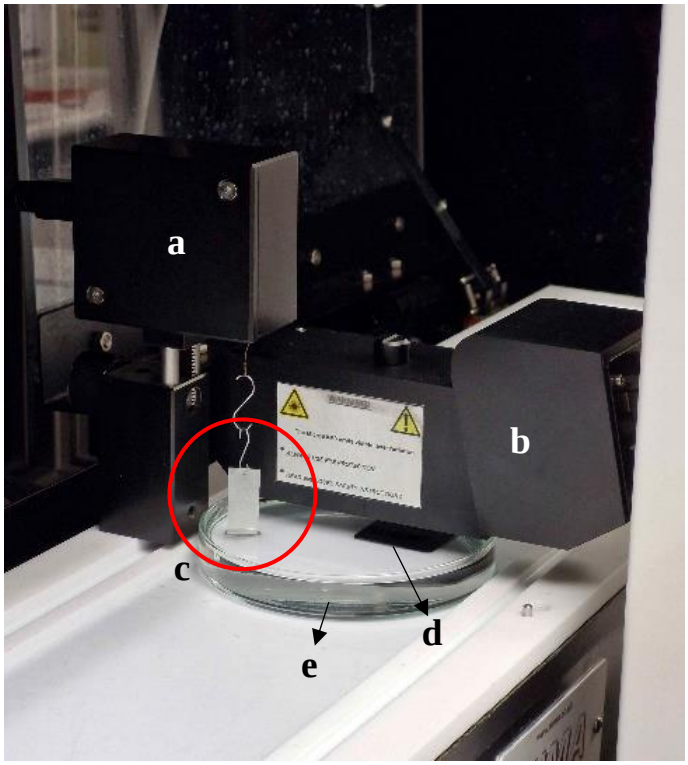

Appendix C

Left panel: π-A isotherms for binary monolayers of GIN-CHOL, GIN-DPPC, GIN-PE, GIN-PS, GIN-PI, and GIN-SM recorded at 21 ºC. **Right panel:** Ks-π plots for GIN-CHOL, GIN-DPPC, GIN-PE, GIN-PS, GIN-PI, and GIN-SM binary systems.

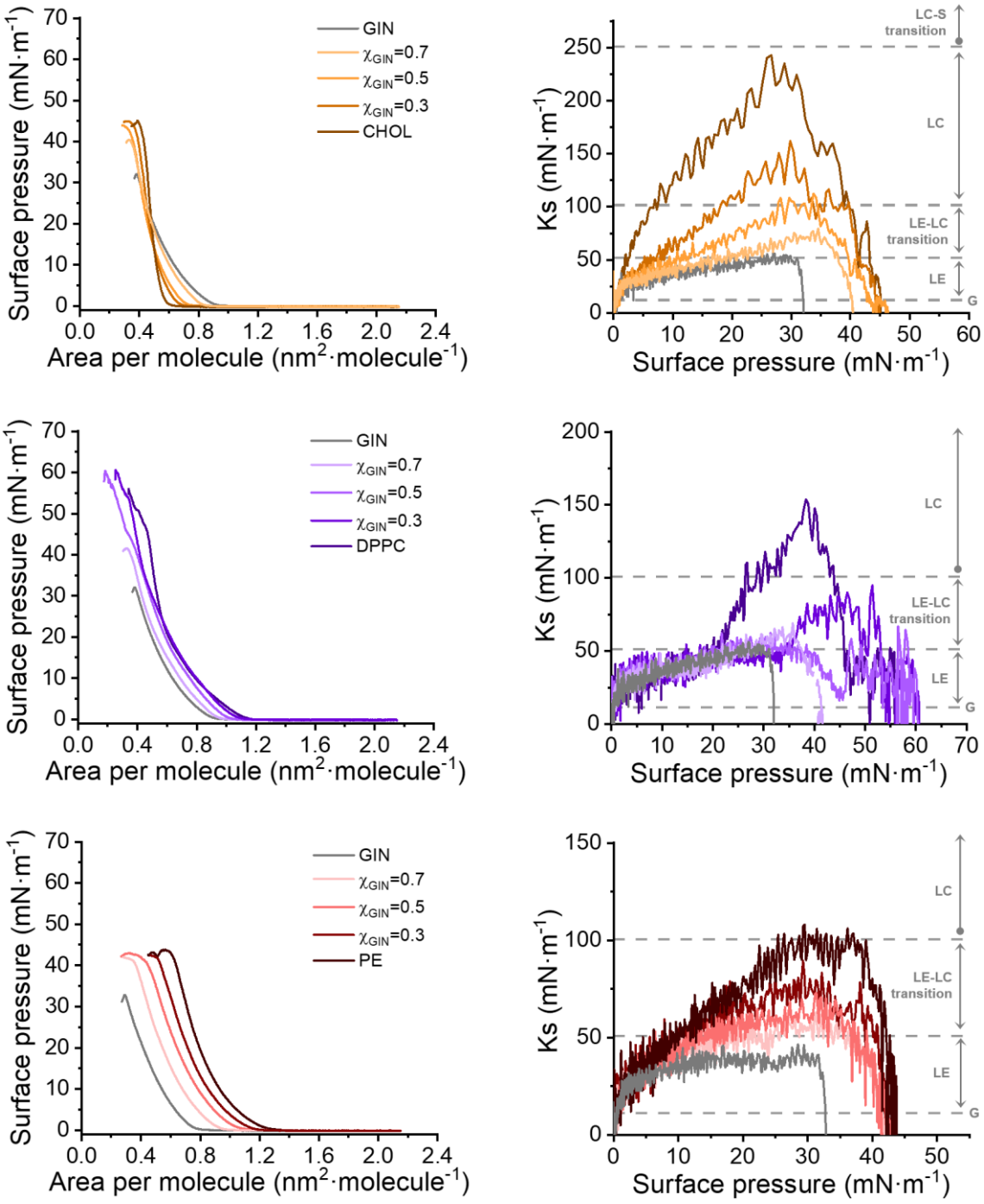

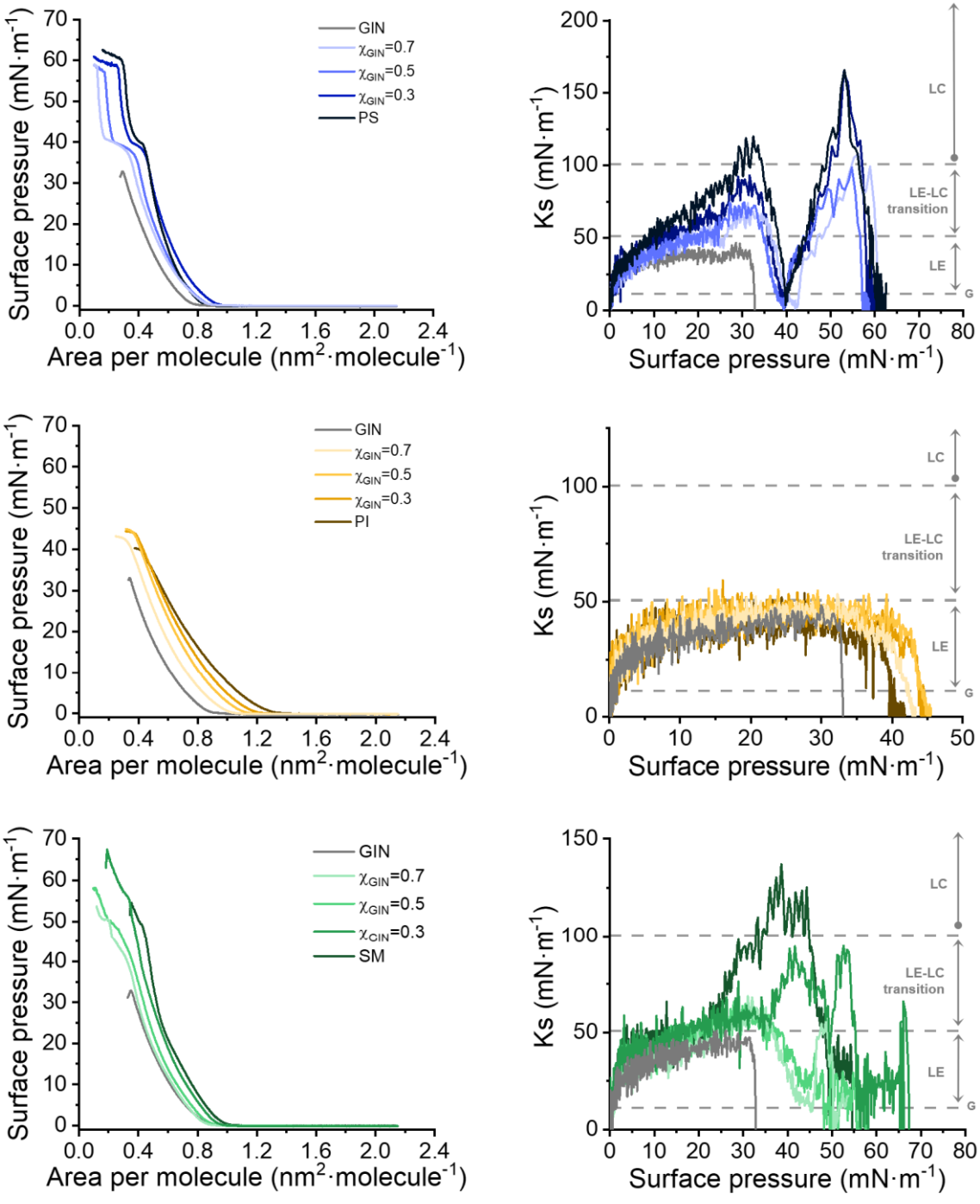
Surface pressure (mN·m-1)
Area per molecule (nm2·molecule-1)
GIN
χGIN=0.7
χGIN=0.5
χGIN=0.3
PS
Ks (mN·m-1)
Surface pressure (mN·m-1)
LC
LE-LC transition
LE
G
GIN
χGIN=0.7
χGIN=0.5
χGIN=0.3
PI
GIN
χGIN=0.7
χGIN=0.5
χGIN=0.3
SM

Appendix D

Left panel: π-A isotherm of the healthy and the IBD-affected membrane registered in the stability experiments at a target surface pressure of 30 $mN \cdot m^{-1}$. **Right panel:** Area per molecule reduction expressed as the area per molecule at a certain time, A, divided by the initial area per molecule achieved at the target surface pressure, A_0, during the stability studies of the healthy and the disturbed membrane.